Soil Biology and Biochemistry 202 (2025) 109698

Contents lists available at ScienceDirect

Soil Biology and Biochemistry

journal homepage: www.elsevier.com/locate/soilbio

Trait-based modeling of microbial interactions and carbon turnover in the rhizosphere

Ahmet Kürşad Sırcan [a,*], Thilo Streck [a], Andrea Schnepf [b,c], Mona Giraud [b,c], Adrian Lattacher [d], Ellen Kandeler [d], Christian Poll [d], Holger Pagel [b,c]

[a] University of Hohenheim, Institute of Soil Science and Land Evaluation, Department of Biogeophysics, Germany
[b] Forschungszentrum Jülich GmbH, Institute of Bio- and Geosciences IBG-3: Agrosphere, Germany
[c] University of Bonn, Institute of Crop Science and Resource Conservation, Germany
[d] University of Hohenheim, Institute of Soil Science and Land Evaluation, Department of Soil Biology, Germany

ARTICLE INFO

Keywords:
Trait-based rhizosphere modeling
Rhizodeposition legacy
Spatial microbial patterns
Constraint-based parameter sampling

ABSTRACT

Understanding the feedback mechanisms between roots and soil, and their effects on microbial communities, is crucial for predicting carbon cycling processes in agroecosystems. Process-based modeling is a valuable tool for quantifying biogeochemical processes and identifying regulatory mechanisms in the rhizosphere. A novel one-dimensional axisymmetric rhizosphere model is used to simulate the spatially resolved dynamics of microorganisms and soil organic matter turnover around a single root segment. The model accounts for two functional groups with different life history strategies (copiotrophs and oligotrophs), reflecting trade-offs in functional microbial traits related to substrate utilization and microbial metabolism. It considers differences in the accessibility of soil organic matter by including the microbial utilization of low and high molecular weight organic carbon compounds (LMW-OC, HMW-OC). The model was conditioned using Bayesian inference with constraint-based parameter sampling, which enabled the identification of parameter sets resulting in plausible model predictions in agreement with experimental evidence.

Mimicking the behavior of growing roots, the model assumed 15 days of rhizodeposition for LMW-OC. The simulations show a decreasing pattern of dissolved LMW-OC away from the root surface. We observed a dominance of copiotrophs close to the root surface (0–0.1 mm). Spatial patterns of functional microbial groups persisted after rhizodeposition ended, indicating a legacy effect of rhizodeposition on microbial communities, particularly on oligotrophic activity. Simulated microbial biomass exhibits a very rapid change within 0–0.2 mm away from the root surface, which points to the importance of resolving soil properties and states at sub-millimeter resolution. Microbial-explicit rhizosphere modeling thus facilitates elucidating spatiotemporal patterns of microorganisms and carbon turnover in the rhizosphere. The identified legacy effect of rhizodeposition on soil microorganisms might be leveraged for rhizosphere-based carbon stabilization strategies in agroecosystems.

1. Introduction

The rhizosphere, the soil region surrounding plant roots, is significantly influenced by root activity (Clark, 1949; Hinsinger et al., 2009; Russell, 1978). The rhizosphere typically extends from less than 1 mm to 1 cm from the root surface into the surrounding soil (Schenck zu Schweinsberg-Mickan et al., 2012), although this range can vary based on several factors, including plant species, soil type, and environmental conditions. Rhizodeposition, which involves the release of organic compounds such as sugars, amino acids, organic acids, and dead root cells, is crucial for shaping the rhizosphere environment. These compounds serve as substrates for microbial metabolism, supporting diverse microbial communities and significantly elevating microbial abundance in the rhizosphere compared to bulk soil (Blagodatskaya et al., 2021; Hartmann et al., 2009). Despite its importance, predicting the spatial and temporal patterns of microbial abundance influenced by rhizodeposition remains challenging due to the complexity of rhizosphere interactions. Process-based modeling has emerged as a powerful tool in

* Corresponding author.
E-mail address: ahmet.sircan@uni-hohenheim.de (A.K. Sırcan).

https://doi.org/10.1016/j.soilbio.2024.109698
Received 17 June 2024; Received in revised form 9 December 2024; Accepted 16 December 2024
Available online 21 December 2024

addressing these challenges, providing insights into microbial community dynamics, organic matter turnover, and nutrient availability (König et al., 2020; Kuppe et al., 2022; Schnepf et al., 2022).

In their recent review of rhizosphere modeling approaches, Kuppe et al. (2022) provided a comprehensive framework to simulate various aspects of the rhizosphere, encompassing water flow, solute transport and reaction, rhizodeposition, microbial growth, and the intricate interactions within the microbial community. They summarized that rhizosphere models have successfully simulated diffusion and advection of solute carbon (C), along with a single type of microbial biomass (e.g., Darrah, 1991; Dupuy and Silk, 2016) and sorption (Raynaud, 2010; Szegedi et al., 2008). More ecologically oriented models have provided a more detailed representation of microbial C at higher temporal resolution (Faybishenko and Molz, 2013; Kravchenko et al., 2004; Raynaud et al., 2006; Strigul and Kravchenko, 2006; Zelenev et al., 2006). Yet, most of the microbial rhizosphere models have considered microbial biomass as a single pool, neglecting the diversity of microorganisms that is expressed in their differing physiological traits (Darrah, 1991; Dupuy and Silk, 2016; Scott et al., 1995). Analogously, the models that considered microbial diversity neglected the spatial variation of microbial biomass in the rhizosphere (Faybishenko and Molz, 2013; Strigul and Kravchenko, 2006; Zelenev et al., 2006).

The functional traits of soil microorganisms determine how individual microorganisms and microbial communities respond to C and nutrient availability and how they utilize organic compounds (Fatichi et al., 2019; Hellweger et al., 2016; Wieder et al., 2015). Malik et al. (2020) categorized microbial communities into different groups based on their life history strategies, characterized by sets of traits that are interrelated due to physiological trade-offs. These strategies allow for the classification of microbial communities along a continuum that may be bimodal to trimodal. The bimodal classification typically includes r-strategists, characterized by a short life expectancy and rapid reproduction, and K-strategists, which have a longer life expectancy and lower reproductive capacity (Fierer et al., 2012; Lauro et al., 2009). These microbial communities are often labelled copiotrophic and oligotrophic, respectively (Fierer et al., 2012). Considering these life history strategies can help predict how different microbial communities respond to changing environmental conditions and resource availability.

Nuccio et al. (2020) demonstrated that microbial diversity within rhizosphere microorganisms is not only high but also spatially and temporally regulated, which supports coexistence and niche differentiation. Additionally, an experimental study highlighted the role of growth rate traits in rhizosphere microorganisms, showing that nutrient availability can stimulate the population of fast-growing bacteria while leading to an increase in slow-growing bacteria under nutrient-poor conditions (Blagodatskaya et al., 2014). Incorporating these insights into a modeling framework for the rhizosphere can enhance our ability to predict stress responses and the impact on nutrient uptake by plants (Dupuy and Silk, 2016).

Spatiotemporal distributions of copiotrophic (r-strategists) and oligotrophic (K-strategists) microorganisms have been simulated by different mathematical models in soil systems (Pagel et al., 2020; Wieder et al., 2015). There is currently a lack of mathematical models that account for spatial changes in microbial biomass and organic carbon as a function of distance from the root surface while also incorporating life history strategies in the rhizosphere. Developing such a model poses significant challenges, primarily related to the parameterization of microbial traits and the model validation process. Both are hindered by the limited availability of experimental data.

Recent research in 16S rDNA amplicon sequencing, which is used to determine microbial species in the rhizosphere, have the potential to address these challenges. Studies have indicated that the copy number of rrn operons in a microorganism's genome, is associated with various functional traits of microorganisms, such as growth rate and Carbon Use Efficiency (Roller et al., 2016). Microorganisms with high rrn copy numbers are typically associated with copiotrophs, while those with a low number of rrn copies tend to be oligotrophs (Bledsoe et al., 2020; Bulgarelli et al., 2013; Matthews et al., 2019; Zarraonaindia et al., 2015). Ling et al. (2022) investigated rrn copy numbers based on 557 pairs of published 16S rDNA amplicon sequence data from different ecosystems worldwide. They reported that the rhizosphere exhibited 6.6% more rRNA operon counts than the bulk soil, suggesting a preference for the fast-growing bacteria (copiotrophs) in the rhizosphere rather than bulk soil.

In light of all the recent research on microbial classification in the rhizosphere, we aim to explore how rhizodeposition influences the spatiotemporal distribution of microbial functional groups in the rhizosphere. We anticipate a higher copiotrophic biomass compared to that of oligotrophs near the root surface. It is however unclear how their concentrations and gradients will be affected by varying rhizodeposition rates associated to different root ages. For low molecular weight organic C compounds (LMW-OC), rhizodeposition of a growing root is much higher at the root tips and a few centimeters behind compared to the older part of the root (Landl et al., 2021a). At a location, through which the root has grown, rhizodeposition will therefore considerably decrease with time. Estimating the spatiotemporal patterns of microorganisms can offer insights into the rhizodeposition legacy effect, which shows the enduring influence of plant roots on the soil environment even after organic C release has ended. This effect significantly shapes subsequent root development through various mechanisms, such as the enrichment of beneficial (positive effect on plant growth) or pathogenic (negative effect on root development) microorganisms (Hu et al., 2018; Philippot et al., 2013) and microbial-plant nutrient competition (Bledsoe et al., 2020; López et al., 2023). Despite this, there exists limited knowledge regarding the persistence of these legacy effects on soil microorganisms under the influence of rhizodeposition (Nannipieri et al., 2023).

In this study, we have developed a process-based model that simulates the distribution of two diverse microbial functional groups and C turnover in the rhizosphere. We incorporated the structure of a bimodal (oligotrophs-copiotrophs) trait-based soil organic matter model (Pagel et al., 2020) in a 1-D axisymmetric rhizosphere model to simulate the effect of rhizodeposition on these microbial functional groups. Adaptation of microorganisms to nutrient stress environments is simulated assuming two different states for each microbial group: active and dormant. Since microbially explicit models typically show equifinality (Marschmann et al., 2019) and measured data are often not yet informative enough to calibrate such trait-based models, our study applies a Bayesian model-conditioning method that leverages evidence-based knowledge derived from measurements to constrain the parameter space of the model such that it yields reliable predictions of microbial dynamics and C flow in the rhizosphere (Chavez Rodriguez et al., 2022). At the end, sensitivity analysis was performed to identify the most influential parameters affecting microbial legacy. The duration of legacy effects for two different microbial functional groups in the rhizosphere was estimated and compared under low and high rhizodeposition scenarios.

2. Methods

2.1. Rationale and concept

The **TraiRhizo** model simulates carbon (C) and microbial dynamics in a soil cylinder around an individual root (Fig. 1A). Consistent with other rhizosphere modeling approaches (Dupuy and Silk, 2016; Darrah, 1991) and in line with experimental evidence showing a typical rhizosphere extent of 0.5–4 mm (Kuzyakov and Razavi, 2019), we used a fixed rhizosphere radius of $r_r = 2$ mm. While the radius r_b defines the outer domain boundary of the model, the radius r_r defines the rhizosphere extent used to calculate process constraints for model parameterizion. The model considers a one-dimensional (1D) axisymmetric domain in cylindrical coordinates. In line with the soil continuum

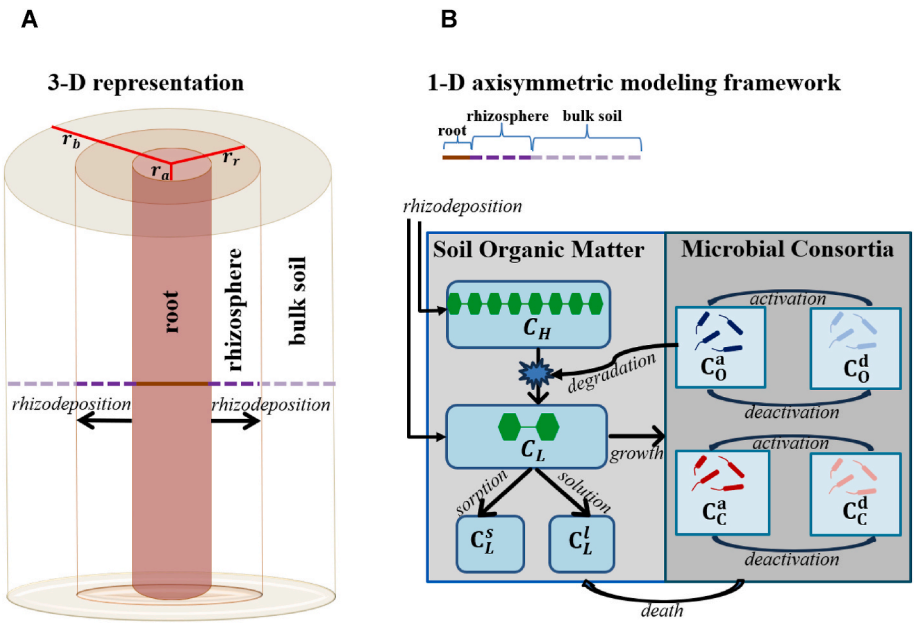

Fig. 1. Model structure **A)** 3D visualization of the root free and root influenced soil with 1D axisymmetric representation of the modeled domain **B)** model carbon pools and their interactions in the 1D axisymmetric modeling framework.

concept of soil organic matter cycling (Lehmann et al., 2020) and similar to the conceptualization in the 2D spatially explicit trait-based soil C cycling model SpatC (Pagel et al., 2020). TraiRhizo distinguishes oligotrophs (C_O) and copiotrophs (C_C) (Fig. 1B). These strategies are reflected in the parameterization of trade-offs between functional traits representing functional characteristics of microbial populations similar to existing trait-based soil C cycling models (Wieder et al., 2015). The model additionally reflects the physiological adaptation of microorganisms to limited C supply by considering dynamic shifts between active (C_O^a, C_C^a) and dormant (C_O^d, C_C^d) physiological states (Fig. 1B).

TraiRhizo distinguishes two C pools with respect to their assimilability by microorganisms (Fig. 1B). Rhizodeposition is represented in the model as a constant input of these two organic C pools from the root to the soil. While high-molecular-weight organic C compounds (C_H) represent organic compounds with a high molecular mass (≥600 Da) that cannot be taken up by microorganisms directly, low-molecular-weight organic C compounds (C_L) stand for organic molecules with a low molecular mass (<600 Da), which can be taken up into microbial cells (Lehmann and Kleber, 2015). We assume high-molecular-weight organic carbon compounds can be transformed to low-molecular-weight organic carbon compounds by extracellular enzymes of oligotrophs. While extracellular enzymes are not represented as a state variable in the model, this transformation process is controlled by the abundance of active oligotrophs (eqn. (15)). The model considers dissolved and sorbed low-molecular-weight organic C compounds (C_L^l, C_L^s). Only dissolved low-molecular-weight organic C compounds are directly accessible for microorganisms.

2.2. Governing equations

TraiRhizo is formulated as a coupled system of partial and ordinary differential equations. Section 2.2.1 and 2.2.2 introduces the state variables (Table 1) and corresponding governing equations describing their dynamics. Mathematical formulations of process rate expressions (F) and functions are given in section 2.2.3 (Table 2). Descriptions, units and ranges of parameters are summarized in Tables 3 and 4.

2.2.1. Soil organic matter

The dynamics of soil organic matter pools is given by the following mass balances, transport and transformation processes:

High-molecular-weight organic C compounds

$$\theta\frac{\partial C_H}{\partial t} = -F_{depoly} + p_H F_{decay} + \frac{\partial}{\partial r}\left(\mathrm{D_H}\left(\theta\right)\frac{\partial \mathrm{C_H}}{\partial r}\right) + \frac{1}{r}\mathrm{D_H}\left(\theta\right)\frac{\partial C_H}{\partial r} \quad (1)$$

Low-molecular-weight organic C compounds

$$\theta R\frac{\partial C_L^l}{\partial t} = F_{depoly} - \frac{1}{Y_O}F_{growth,O} - \frac{1}{Y_C}F_{growth,C} + (1-p_H)\,F_{decay} - F_{uptake,L} - \rho_B\,F_{sorp} + \frac{\partial}{\partial r}\left(\mathrm{D_L}(\theta)\frac{\partial C_L^l}{\partial r}\right) + \frac{1}{r}\mathrm{D_L}(\theta)\frac{\partial C_L^l}{\partial r} - \overline{q_{wr}}\frac{\partial C_L^l}{\partial r} \quad (2)$$

where θ is the volumetric water content, p_H is the proportion of high-molecular-weight organic C compounds (HMW-OC) formed from dead

Table 1
Model pools and initial conditions.

Variable	Definition	Unit	Initial concentration
C_H	Concentration of high-molecular-weight organic C compounds in soil	mg cm^{-3}solution	7–14
C_L^l	Concentration of dissolved low-molecular-weight organic C compounds in soil solution	mg cm^{-3}solution	0.0001-0.04
$C_L^{s,2}$	Sorbed concentration of low-molecular-weight organic C compounds in sorption region two	mg g^{-1} solid	0.0001-0.5
C_O^a	Concentration of active oligotrophs	mg cm^{-3} soil	0–0.003
C_C^a	Concentration of active copiotrophs	mg cm^{-3} soil	0–0.003
C_O^d	Concentration of dormant oligotrophs	mg cm^{-3} soil	0.11-0.12
C_C^d	Concentration of dormant copiotrophs	mg cm^{-3} soil	0.11-0.16
C_{CO_2}	Concentration of carbon dioxide	mg cm^{-3} soil	0.11-0.18

* All state variables are expressed in mass-based units of C and they are expressed per soil volume for microbial consortia, per soil mass for sorbed C pools ($C_L^{s,1}$; $C_L^{s,2}$), and per solution volume for the rest of the organic C pools (C_H, C_L^l).

Table 2
Process rates and functions.

Internal flows	Definition	Unit
F_{depoly}	Depolymerization of high-molecular-weight organic C compounds to low-molecular-weight organic C compounds	mg cm^{-3} d^{-1}
F_{decay}	Total microbial decay due to endogenous maintenance	mg cm^{-3} d^{-1}
$F^{j}_{decay,i}$	Decay of the corresponding microbial group i with i = {O,C} in the corresponding metabolic state j with j = {active, dormant}	mg cm^{-3} d^{-1}
$F_{growth,i}$	Growth of the corresponding microbial group i with i = {O,C} on low-molecular-weight organic C compounds	mg cm^{-3} d^{-1}
$F_{deact,i}$	Deactivation of the corresponding microbial group i with i = {O,C}	mg cm^{-3} d^{-1}
$F_{react,i}$	Reactivation of the corresponding microbial group i with i = {O,C}	mg cm^{-3} d^{-1}
$F_{uptake,L}$	Total microbial uptake of low-molecular-weight organic C compounds	mg cm^{-3} d^{-1}
$F^{j}_{uptake,L,i}$	Specific microbial uptake of low-molecular-weight organic C compounds by group i with i = {O,C} in metabolic state j with j = {active, dormant}	mg cm^{-3} d^{-1}
$F^{j}_{maintanence,i}$	Total maintenance requirements of the corresponding microbial group i with i = {O,C} in the corresponding metabolic state j with j = {active, dormant}	mg cm^{-3} d^{-1}
F_{sorp}	Sorption of dissolved low-molecular-weight organic C compounds	mg cm^{-3} d^{-1}

microbial biomass, R is the retardation factor (see Appendix 1.2.2 for the derivation), Y_O and Y_C denote growth yields of oligotrophs and copiotrophs, and ρ_B is the bulk density of soil.

Transport of LMW-OC (eqn. (2)) is described by the advection-diffusion equation within a 1D axisymmetric coordinate system (see Appendix 1.1 for the complete derivation). To account for typical characteristics of gel-like mucilage released from roots, TraiRhizo assumes slow diffusion of HMW-OC in soil and neglects convective transport. Carbon input via rhizodeposition is defined by the corresponding boundary conditions (eqns. (27) and (28)).

The radial flux ($\overline{q_{wr}}$) is determined by the radial flux at the root surface (q_{wr_a}) and decreases proportionally with the ratio of the root cylinder radius (r_a) to the radial distance from the root center (r) (see Appendix 1.3 for the derivation):

$$\overline{q_{wr}} = -q_{wr_a}\frac{r_a}{r} \tag{3}$$

The apparent diffusion coefficient is given by (Millington and Quirk, 1961):

$$\mathrm{D_i}(\theta) = D_{i,w}\left(\frac{\theta^{\frac{10}{3}}}{\varphi^2}\right) \; for \; i = H, L \tag{4}$$

where $D_{H,w}$ and $D_{L,w}$ are the diffusion coefficient in pure water for HMW-OC and LMW-OC, respectively. Soil porosity (φ) is defined as:

$$\varphi = 1 - \frac{\rho_B}{\rho_S} \tag{5}$$

2.2.2. Microbial consortia

Microbial concentrations change due to growth, deactivation, reactivation and decay processes:

Active oligotrophs

$$\frac{\partial C^a_O}{\partial t} = F_{growth,O} - F_{deact,O} + F_{react,O} - \frac{1}{Y}F^a_{decay,O} \tag{6}$$

Active copiotrophs

$$\frac{\partial \mathrm{C^a_C}}{\partial \mathrm{t}} = \mathrm{F_{growth,C}} - \mathrm{F_{deact,C}} + \mathrm{F_{react,C}} - \frac{1}{Y}\mathrm{F^a_{decay,C}} \tag{7}$$

Table 3
Model parameters and their defined ranges.

Parameters	Definition	Unit	Initial Interval	Source
Geometry				
r_a	Radius of root cylinder	cm	10^{-3}-10^{-1}	1 2 3
r_b	Radius of soil cylinder	cm	1–10	no impact
$J_{L,root}$	Root-released flux of low-molecular-weight organic C compounds	mg cm^{-2}d^{-1}	10^{-3}-3. 10^{-1}	4 5 6
$J_{H,root}$	Root-released flux of high-molecular-weight organic C compounds	mg cm^{-2}d^{-1}	10^{-3}-3. 10^{-1}	6
Soil organic matter				
p_H	Proportion of high-molecular-weight organic C compounds formed from microbial biomass due to decay by endogenous maintenance	1	0–1	full range
$V_{max,H}$	Maximum reaction rate of enzymes targeting high-Molecular-weight organic C compounds	d^{-1}	10^{-3}-1	7
K_H	Half-saturation coefficients of enzymes targeting high-molecular-weight organic C compounds	mg cm^{-3}	10^{-6} - 10	7
$D_{L,W}$	Diffusion coefficient of low-molecular-weight organic C compounds in water	cm^2d^{-1}	10^{-2}-2,5	2 8
$D_{H,w}$	Diffusion coefficient of high-molecular-weight organic C compounds in water	cm^2d^{-1}	0.003456	1
f_{sorp}	Fraction of region 1 sorption sites	1	0.5	13
$C^s_{L,max}$	Maximum sorption capacity	mg g^{-1}	0.0291-1.6925	9 10 11 12
k_P	Langmuir binding coefficient	mg cm^{-3}	0.006-0.25	9 10 11 12
α	Rate coefficient of mass transfer between region 1 and 2 sorption sites	d^{-1}	0.1	13
Soil properties				
ρ_B	Soil bulk density	g cm^{-3}	1–1.6	typically observed in topsoils
ρ_S	Solid phase density	g cm^{-3}	2.650	14
θ	Volumetric soil water content	$\frac{cm^3}{cm^3}$	0.3	fixed
q_{wr_a}	Water flux at root surface	cm d^{-1}	10^{-7}-10	15 16 17
Independent variables				
r	Radial distance from root center	cm		
t	Simulation time	d		

* 1 Landl et al., 2021a 2 Raynaud, 2010 3 Williams and Yanai, 1996 4 Darrah, 1991 5 Kravchenko et al., 2004 6 Chari et al., 2024 7 Pagel et al., 2020 8 Pagel et al., 2016 9 Mayes et al., 2012 10 Jagadamma et al., 2012 11 Jagadamma et al., 2014 12 Kothawala et al., 2009 13 Streck et al., 1995 14 Blake, 2008 15 Norton and Firestone, 1991 16 Von Jeetze et al., 2020 17 Zarebanadkouki et al., 2019.

Dormant oligotrophs

$$\frac{\partial C^d_O}{\partial t} = F_{deact,O} - F_{react,O} - \frac{1}{Y}F^d_{decay,O} \tag{8}$$

Dormant copiotrophs

$$\frac{\partial C^d_C}{\partial t} = F_{deact,C} - F_{react,C} - \frac{1}{Y}F^d_{decay,C} \tag{9}$$

where Y denotes the maintenance yield. Total CO_2-production (i.e.,

Table 4
Model parameters and their defined ranges.

Microbial consortia					
Parameters	Definition	Unit	Microbial group i = O	Microbial group i = C	Source, remark
$\mu_{max,i}$	Maximum growth rate coefficient for the corresponding microbial group i with i = {O,C}	d^{-1}	10^{-2}-10	10^{-1}-100	7
$k_{i,L}$	Specific substrate affinity to low-molecular-weight organic C compounds for microbial group i with i = {O,C}	$cm^3\ mg^{-1}\ d^{-1}$	1–500	1–500	8
Y_i	Growth yield on low-molecular-weight organic C compounds for the corresponding microbial group i with i = {O,C}	$\frac{mg(C)}{mg(C)}$	0–1	0–1	full range
$m_{max,i}$	Maximum maintenance rate coefficient for the corresponding microbial group i with i = {O,C}	d^{-1}	10^{-5}-2	10^{-5}-2	8
β_i	Reduction factor of maintenance requirements in dormant state for the corresponding microbial group i with i = {O,C}	1	10^{-2}-1	10^{-4}-1	7 18 19
$k_{d,i}$	Deactivation rate coefficient for the corresponding microbial group i with i = {O,C}	d^{-1}	10^{-2}-100	10^{-2}-100	7 20
$k_{r,i}$	Reactivation rate coefficient for the corresponding microbial group i with i = {O,C}	d^{-1}	10^{-2}-100	10^{-2}-100	7 20
$C_{thres,i}$	Threshold concentration for reactivation and deactivation for the corresponding microbial group i with i = {O,C}	$mg\ cm^{-3}$	3. 10^{-7}-0.3	3. 10^{-7}-0.3	7
Y	Maintenance yield	1	0–1		full range
a	Sharpness parameter for the switch function from active to dormancy	1			7

* 18 Wieder et al., 2015 19 Zhang et al., 2022 20 Stolpovsky et al., 2011.

respiration) follows from the C mass balance:

$$\frac{\partial C_{CO_2}}{\partial t} = \frac{1-Y_O}{Y_O} F_{growth,O} + \frac{1-Y_C}{Y_C} F_{growth,C} + \frac{1-Y}{Y} F_{decay} + F_{uptake,L} \quad (10)$$

2.2.3. Process rates and functions

2.2.3.1. Sorption. The amount of sorbed C might alter the distribution of microbial groups, which have distinct strategies dependent on substrate availability. In the defined model parameter space (Tables 3 and 4), the linear sorption model might not be adequate to reflect the sorption isotherm precisely enough (Streck et al., 1995). Unlike in most other rhizosphere models (Darrah, 1991; Nye and Marriott, 1969; Raynaud, 2010), the sorption of LMW-OC from soil solution is represented by a nonlinear sorption model. This model uses a two-stage one-rate approach, considering two sorption regions of different accessibility (Streck et al., 1995). While the sorption sites in region 1 are in direct contact with the soil solution, region 2 sites exchange only with region 1 sites. Sorption of LMW-OC from soil solution to region 1 sorption sites is reflected as an equilibrium process. Mass transfer from region 1 to region 2 sorption sites occurs as a kinetic process, probably reflecting a diffusion process into the intra-porous space of soil particles.

The total sorbed concentration (C_L^s) is given by:

$$C_L^s = \rho_B f_{sorp} C_L^{s,1} + \rho_B \left(1 - f_{sorp}\right) C_L^{s,2} \quad (11)$$

where f_{sorp} is the fraction of region 1 sorption sites. The variables $C_L^{s,1}$ and $C_L^{s,2}$ stand for sorbed concentrations in regions 1 and 2, respectively. Equilibrium sorption at region 1 sites follows a Langmuir isotherm (Swenson and Stadie, 2019):

$$C_L^{s,1} = C_{L,max}^s \frac{C_L^l}{k_P + C_L^l} \quad (12)$$

$C_{L,max}^s$ represents the maximum sorption capacity of LMW-OC, while k_P denotes the Langmuir constant. The change of concentration of sorbed LMW-OC in region 2 is given by:

$$\frac{\partial C_L^{s,2}}{\partial t} = \frac{1}{1-f_{sorp}} F_{sorp} \quad (13)$$

Kinetic sorption is described as mass transfer from region 1 to region 2 sites:

$$F_{sorp} = \alpha \left(C_L^{s,1} - C_L^{s,2}\right) \quad (14)$$

where α is a rate coefficient.

2.2.3.2. Microbial processes. Active oligotrophs catalyze the depolymerization of HMW-OC according to Michaelis–Menten kinetics (cf. Pagel et al., 2020):

$$F_{depoly} = v_{max,H} \frac{C_H}{K_H + C_H} C_O^a \quad (15)$$

where $v_{max,H}$ is the maximum reaction rate and K_H is the half saturation constant.

Microbial growth, decay, activation and inactivation follow the formulations of the SpatC model with small modifications (Pagel et al., 2020):

$$F_{decay} = F_{decay,O}^a + F_{decay,C}^a + F_{decay,O}^d + F_{decay,C}^d \quad (16)$$

$$F_{decay,i}^j = F_{maintanence,i}^j - F_{uptake,L,i}^j \quad (17)$$

Where the index i represents oligotrophs (O) or copiotrophs (C), and the index j represents active (a) or dormant (d).

In eqn. (17), the first term on the RHS represents total maintenance requirements ($F_{maintanence,i}^j$) and the second term represents the uptake of LMW-OC for exogenous maintenance $\left(F_{uptake,L,i}^j\right)$. The difference between both flows defines microbial decay ($F_{decay,i}^i$) as a result of endogenous maintenance.

The following equations define total maintenance requirements:

$$F_{maintanence,i}^a = m_{max,i} C_i^a \quad (18)$$

$$F_{maintanence,i}^d = m_{max,i} \beta_i C_i^d \quad (19)$$

where $m_{max,i}$ is the maximum maintenance requirement for each microbial group and β_i is the reduction factor for the dormant state.

The uptake of LMW-OC for exogenous maintenance and microbial growth on LMW-OC according to Monod kinetics is given by:

$$F_{uptake,L} = F_{uptake,L,O,a} + F_{uptake,L,C,a} + F_{uptake,L,O,d} + F_{uptake,L,C,d} \quad (20)$$

$$F_{uptake,L,i}^a = \frac{m_{max,i} C_L^l k_{i,L}}{m_{max,i} + C_L^l k_{i,L}} C_i^a \quad (21)$$

$$F_{uptake,L,i}^d = \frac{m_{max,i} C_L^l k_{i,L}}{m_{max,i} + C_L^l k_{i,L}} \beta_i C_i^d \quad (22)$$

$$F_{growth,i} = \frac{\mu_{max,i}\, C_L^l\, k_{i,L}}{\mu_{max,i} + C_L^l\, k_{i,L}} C_i^a \quad (23)$$

where $k_{i,L}$ represents the specific substrate affinity and $\mu_{max,i}$ is the specific growth rate for each microbial group (i = O,C).

Activation and inactivation follow first-order kinetics:

$$F_{deact,i} = (1 - \phi_i)\, k_{d,i} C_i^a \quad (24)$$

$$F_{react,i} = \phi_i k_{r,i} C_i^d \quad (25)$$

Here ϕ_i is the switch function between two states of microorganisms and defined as:

$$\phi_i = \frac{1}{\exp\left(\frac{C_{thres,i} - C_L^l}{a\, C_{thres,i}}\right) + 1} \quad (26)$$

where $C_{thres,i}$ is the threshold concentration of dissolved LMW-OC for deactivation and reactivation, and a reflects the sharpness of the transition between states (Pagel et al., 2020) for each microbial group (i = O, C).

2.2.4. Boundary conditions

The duration of rhizodeposition was set to 15 days for LMW-OC and 9 days for HMW-OC. Landl et al. (2021b) simulated rhizodeposition hotspot for mucilage and citrate in a growing root system. The maximum values from the simulation results for the duration of rhizodeposition hotspots were used. However, a reasonable range for the total amount of rhizodeposited C was derived based on an extensive literature search (Table 3).

We used a Cauchy boundary condition to prescribe C flux at the root soil interface ($r = r_a$):

2.2.4.1. Low-molecular-weight organic C compounds

$$-\mathrm{D_L}(\theta)\, \frac{\partial C_L^l}{\partial r} + \overline{q_{wr}} C_L^l \Big|_{r=r_a} = J_{L,root}(t) \quad (27)$$

2.2.4.2. High-molecular-weight organic C compounds

$$-\mathrm{D_H}(\theta)\, \frac{\partial C_H}{\partial r}\Big|_{r=r_a} = J_{H,root}(t) \quad (28)$$

All simulations assume zero flux at the outer boundary ($r = r_b$). Similar to the assumption in Raynaud (2010), the soil radius for a root was chosen to be sufficiently large (see Table 3) to safely assume that there is no impact on the adjacent root.

2.3. Model implementation and programming

The model equations were solved using COMSOL multiphysics 5.5 with MATLAB R2020b by using adaptive time steps, adjusting maximum time step to 0.1 d (Pagel et al., 2020; Schwarz et al., 2022). All pre- and post-processing and parameter sampling was done using the MATLAB Livelink (communication protocol between COMSOL and MATLAB via JAVA) feature.

2.3.1. Model initialization

A 100-day spin-up simulation period without rhizodeposition and root water uptake was run to initialize all state variables to steady-state values. After this spin-up, the simulations considered active root deposition and root water uptake. To initialize the spin-up simulations, initial values from a microbial explicit soil organic model (SpatC) were applied as initial conditions (Pagel et al., 2020). For spin-up simulations, initial values of LMW-OC at region 2 sorption sites ($C_S^{s,2}$) were assumed to be in equilibrium with region 1 sorption sites ($C_S^{s,2} = C_S^{s,1}$)

2.4. Model parametrization: constraint-based Markov Chain Monte Carlo parameter sampling method

We applied a constrained-based Markov Chain Monte Carlo (cb MCMC) parameter sampling method (Chavez Rodriguez et al., 2022) to derive representative posterior parameter distributions for the TraiR-hizo model. These distributions reflect the viable parameter space (Zamora-Sillero et al., 2011) in a way that leads to predictions of characteristic system behavior. Briefly, the method leverages experimental evidence by formulating parameter and process constraints which formalize the current knowledge and understanding of model parameterization and system behavior. The cb MCMC method ensures that preset quantitative equality and inequality relationships between parameters are maintained. Moreover, it also ensures such relationships between model outputs. The cb MCMC method uses an iterative algorithm that successively increases the number of parameter and process constraints to efficiently explore the viable parameter space. We defined 13 parameter constraints (Table 5) and 9 process constraints (Tables 6 and 7). These constraints were derived from a literature analysis of the existing experimental evidence on rhizosphere processes and their controls.

2.4.1. Parameter constraints

Parameter constraints related to microbial physiology and substrate usage were defined according to a bimodal life history strategy scheme, which distinguishes between copiotrophs and oligotrophs (Treseder, 2023). While copiotrophs are characterized by higher metabolic rates, oligotrophs are characterized by higher substrate affinity and growth yield. The constraints are expressed as relations between biokinetic parameters derived from published experimental data sets and theoretical reflections.

2.4.2. Process constraints

To align with the defined process constraints in experiments, we made a pragmatic choice of a rhizosphere extent (r_r) of 2 mm, a common choice in analogous experimental setups (Kuzyakov and Razavi, 2019). The dynamics of model outputs in rhizosphere and bulk soil was also evaluated based on this definition. The impact of varying r_r values between 0.5 and 2 mm on these distributions was analyzed. The mean

Table 5
Parameter constraints.

	Constraint	Description/Explanation	Source
1.	$\mu_{max,C} > \mu_{max,O}$	Maximum growth rate of copiotrophs is higher than maximum growth rate of oligotrophs.	21 22
2.	$k_{O,L} > k_{C,L}$	Specific substrate affinity to low-molecular-weight organic C compounds for oligotrophs is higher than for copiotrophs.	
3.	$m_{max,C} > m_{max,O}$	Maximum maintenance rate coef. must be higher for copiotrophs than for oligotrophs.	
4.	$C_{thresh,C} > C_{thresh,O}$	Oligotrophs (K-strategists) are adapted to low carbon and nutrient availability.	
5.	$m_{max,i} < \mu_{max,i}$ $i \in \{O,C\}$	This logical constraint ensures that organisms are “fit to survive".	
6.	$k_{r,i} \geq k_{d,i}$ $i \in \{O,C\}$	Transition to dormant (resp. potentially active) state is typically slower than reactivation.	23 24
7.	$k_{j,i} > \mu_{max,i}$ $i \in \{O,C\}$ and $j \in \{r, d\}$	Changes of metabolic state are faster than growth, death, and changes in composition.	23 25
8.	$Y_O > Y_C$	Oligotrophs are slow-growing at high yield, copiotrophs are fast-growing at low yield.	26 27 28

* 21 Blagodatskaya et al., 2009 22 Papp et al., 2020 23 Blagodatskaya and Kuzyakov, 2013 24 Konopka, 1999 25 Salazar et al., 2019 26 Fierer et al., 2007 27 Ho et al., 2017 28 Lipson, 2015.

Table 6
Model outputs used for process constraints.

Variable	Definition	Expression	Unit
MB_R	Mean total microbial biomass in rhizosphere	$\text{mean}_R(C_O^a + C_C^a + C_O^d + C_C^d)$	mg cm^{-3}
MB_B	Mean total microbial biomass in bulk soil	$\text{mean}_B(C_O^a + C_C^a + C_O^d + C_C^d)$	mg cm^{-3}
SOC_R	Mean total organic carbon in rhizosphere	$\text{mean}_R(C_L^l + C_H^l)$	mg cm^{-3}
SOC_B	Mean total organic carbon in bulk soil	$\text{mean}_B(C_L^l + C_H^l)$	mg cm^{-3}
MB_R^a	Mean total active microbial biomass in rhizosphere	$\text{mean}_R(C_O^a + C_C^a)$	mg cm^{-3}
$LMW - DOC_R$	Mean total dissolved low-molecular-weight organic C compounds in rhizosphere	$\text{mean}_R(C_L^l)$	mg cm^{-3}
$LMW - DOC_B$	Mean total dissolved low-molecular-weight organic C compounds in bulk soil	$\text{mean}_B(C_L^l)$	mg cm^{-3}
MB_R^i	Mean total microbial biomass of the corresponding functional group in rhizosphere	$\text{mean}_R(C_i^a + C_i^d)$ where $i \in \{O, C\}$	mg cm^{-3}
MB_B^i	Mean total microbial biomass of the corresponding functional group in bulk soil	$\text{mean}_B(C_i^a + C_i^d)$ where $i \in \{O, C\}$	mg cm^{-3}

concentration over the rhizosphere extent was calculated using the MATLAB mean function, with the error being less than 10% compared to the analytical mean calculation. Each process constraint set is derived from multiple sets of experimental data collected from wheat crops grown in various soil types, textures, root segments, and ages, under differing experimental conditions. At the end, the largest interval found for each metric was defined as a constraint. Table 6 shows the model outputs that were used in setting the process constraints.

3. Results

3.1. Model parameterization using constraint-based Markov Chain Monte Carlo sampling

Conditioning model parameters and outputs with defined constraints, using cb MCMC, resulted in 1647 unique scenarios that fulfill all the parameter and process constraints, referred as fully constrained model simulations. To observe the effect of parameter and process constraints separately, the same number of model simulations fulfilling only the parameter constraints were also calculated. We estimated the posterior distribution of 34 model parameters. Our model introduces a new probability distribution function for each microbial trait-related parameter corresponding to each functional group, based on the fully constrained parameter sets, and compares it with the one derived from the parameter sets which fulfill only parameter constraints (Figs. 2 and 3). To prevent sampling excessively high values within the given interval, each parameter is uniformly sampled on a logarithmic scale.

3.1.1. Parameters related to microbial traits

Parameter constraint 1 (Table 5) informs the model that the maximum growth rate of copiotrophs ($\mu_{max,C}$) is higher than the maximum growth rate of oligotrophs ($\mu_{max,O}$) (Blagodatskaya et al., 2009; Papp et al., 2020), in parallel to parameter constraint 7, which states that $\mu_{max,O}$ and $\mu_{max,C}$ are slower than the changes of metabolic states ($k_{r,O}$, $k_{d,O}$, $k_{r,C}$, $k_{d,C}$) (Blagodatskaya and Kuzyakov, 2013; Salazar et al., 2019). Additionally, parameter constraint 5 ensures that $\mu_{max,O}$ and $\mu_{max,C}$ are faster than the maximum maintenance rate of microorganisms ($m_{max,O}$ and $m_{max,C}$) (Blagodatskaya and Kuzyakov, 2013; Papp et al., 2020). As a result, as seen in the distributions of $\mu_{max,O}$ and $\mu_{max,C}$, the parameter constraints successfully narrow down the corresponding parameter distributions as expected (Fig. 2). The interesting result here is the further shift to lower values in the distributions of $\mu_{max,O}$ (0.01–0.5 d^{-1}) and $\mu_{max,C}$ (0.11–10 d^{-1}) as a result of conditioning the model by process constraints. We also observe an effect of process constraints on decreasing the parameter space of $m_{max,O}$ (<0.01 d^{-1}) and $m_{max,C}$ (<0.1 d^{-1}) by shifting the posterior distribution of the corresponding parameters to lower values (Fig. 2).

Trade-offs in microbial traits such as substrate affinity and yield are addressed through parameter constraints 2 and 8 (Table 5). These constraints inform the model parameters in a way that substrate affinity for oligotrophs ($k_{O,L}$) must be higher than substrate affinity for copiotrophs ($k_{C,L}$) and yield for oligotrophs (Y_O) must be higher than yield for copiotrophs (Y_C) (Blagodatskaya et al., 2009; Fierer et al., 2007; Ho et al., 2017; Lipson, 2015; Papp et al., 2020). The distribution of the corresponding parameters show that parameter constraints successfully condition the corresponding model parameters (Fig. 2). The application of process constraints has a slight effect on the distributions of $k_{O,L}$ and Y_O, shifting to higher values; however, the distributions of $k_{C,L}$ and Y_C reflect significant shifts to higher values in the posterior distributions (Fig. 2), highlighting the importance of process constraints in estimating a more reliable parameter distribution.

Table 7
Defined process constraints.

	Constraint	Description/Explanation	Source
1.	$0.04 < MB_R < 1.2$	The range for the concentration of microbial biomass in the rhizosphere for different soil types, textures, experimental conditions.	29 30 31 32 33 34
2.	$1 < \frac{MB_R}{MB_B} < 2.5$	Microbial biomass is higher in the rhizosphere than bulk soil and lower than a threshold value.	34 35
3.	$4 < SOC_R < 16$	The range for soil organic carbon in the rhizosphere for different soil types, textures, experimental conditions.	32 36
4.	$0.66 < \frac{SOC_R}{SOC_B} < 2$	The range for ratio of soil organic carbon in the rhizosphere to bulk soil for different soil types, textures, experimental conditions.	32 36
5.	$0.0006 < \frac{MB_R^a}{MB_R} < 0.6$	The range for ratio of active microbial biomass to total microbial biomass for different soil types, textures, experimental conditions.	33 37 38 39
6.	$LMW - DOC_R < 0.55$	Based on water extractable organic carbon measurements. Water extractable organic carbon should include dissolved organic carbon (DOC) together with some sorbed carbon mass therefore it must be higher than the DOC concentration.	33 39
7.	$\frac{LMW - DOC_R}{LMW - DOC_B} > 1$	Based on water extractable organic carbon measurements.	33 38
8.	$\frac{MB_R^C}{MB_R^O} > \frac{MB_B^C}{MB_B^O}$	According to 557 pairs of published 16S rDNA amplicon sequences data from the bulk soils and rhizosphere in different ecosystems around the world, it is reported that the rhizosphere had 6.6% more rRNA operon counts, indicating that more fast-growing bacteria (r-strategists) preferentially colonize the rhizosphere than the bulk soil. The rhizosphere was dominated by copiotrophic microorganisms such as Proteobacteria and Bacteroidetes.	40 41
9.	$MB_R^C > MB_R^O$		

* 29 Chen et al., 2015 30 Jin et al., 2022 31 Xu et al., 2019 32 Yang et al., 2013 33 Schenck zu Schweinsberg-Mickan et al., 2012 34 Bonkowski et al., 2000 35 Kuzyakov and Blagodatskaya, 2015 36 Jat et al., 2021 37 Blagodatskaya et al., 2021 38 Fang et al., 2015 39 Li et al., 2013 40 Ling et al., 2022 41 Bledsoe et al., 2020.

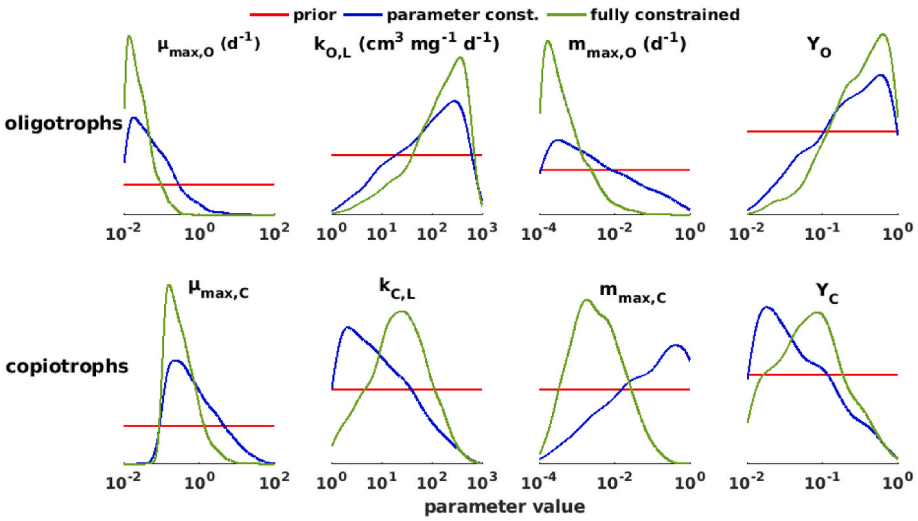

Fig. 2. Comparison of Posterior Model Parameter Distributions, fitted to the Kernel distribution, with Prior Log-Uniform Distributions within a Specified Interval for microbial traits-related parameters. The parameters include growth rate ($\mu_{max,O}, \mu_{max,C}$), substrate affinity ($k_{O,L}, k_{C,L}$), maintenance rate ($m_{max,O}, m_{max,C}$), and growth yield (Y_O, Y_C), presented from right to left for oligotrophs and copiotrophs. The blue curves depict the posterior parameter distributions after applying parameter constraints. The green curves illustrate the parameter distributions after applying both parameter and process constraints. (For interpretation of the references to colour in this figure legend, the reader is referred to the Web version of this article.)

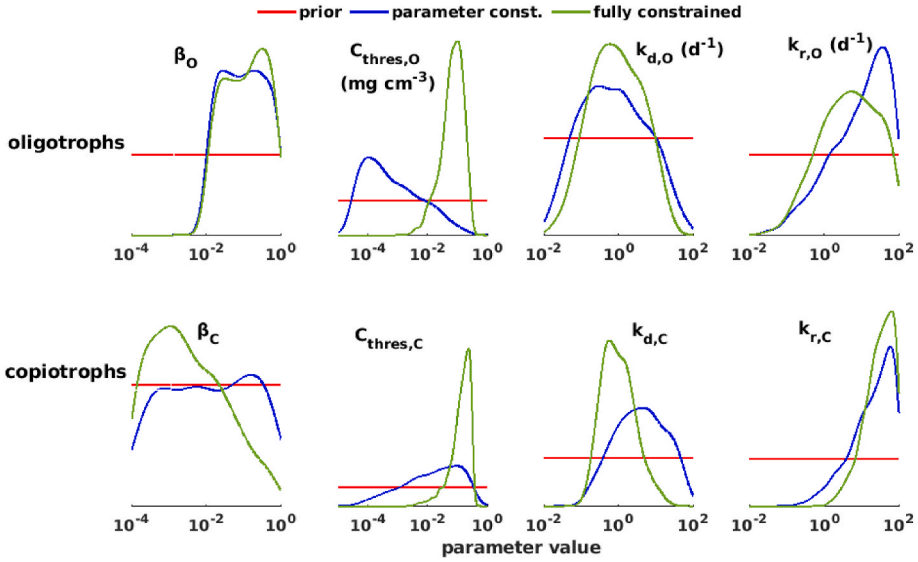

Fig. 3. Comparison of Posterior Model Parameter Distributions, fitted to the Kernel distribution, with Prior Log-Uniform Distributions within a Specified Interval for dormancy traits-related parameters. The parameters include reduction factor in dormancy state (β_O, β_C), threshold substrate concentration for reactivation and activation of microorganisms ($C_{thres,O}, C_{thres,C}$), deactivation rate coefficient ($k_{d,O}, k_{d,C}$), reactivation rate coefficient ($k_{r,O}, k_{r,C}$), presented from right to left for oligotrophs and copiotrophs. The blue curves depict the posterior parameter distributions after applying parameter constraints. The green curves illustrate the parameter distributions after applying both parameter and process constraints. (For interpretation of the references to colour in this figure legend, the reader is referred to the Web version of this article.)

3.1.2. *Parameters related to dormancy strategy*

Cb MCMC successfully constrained most of the microbial parameters related to the dormancy strategy, leading to the estimation of the proportion of dormant biomass in the total microbial biomass near the root (Fig. 6). Parameter constraint 4 specifies that the threshold substrate concentration for the activation of microorganisms will be higher for copiotrophs ($C_{thres,C}$) than for oligotrophs ($C_{thres,O}$) (Blagodatskaya et al., 2009; Papp et al., 2020). The expected shifts based on these constraints are visible in the parameters' distributions (Fig. 3). An interesting result is the significant shift to higher values in the posterior distributions of $C_{thres,C}$ (>0.01 $\frac{mg}{cm^3}$) and $C_{thres,O}$ (>0.004 $\frac{mg}{cm^3}$) when process constraints are applied (Fig. 3). Note that a higher $C_{thres,i}$ indicates a higher substrate concentration in the soil required for microorganisms to be in the active state rather than dormant.

Process constraint 5 informs the model that the proportion of active biomass to total biomass will be less than a threshold value based on several experimental data (Table 7) (Blagodatskaya et al., 2009; Papp et al., 2020). The effects of process constraints here are expected, and the results are consistent with the fact that soil microorganisms are mostly found in a dormant state (Blagodatskaya and Kuzyakov, 2013).

Parameter constraint 6 informs the model that reactivation ($k_{r,O}$, $k_{r,C}$) is generally faster than deactivation ($k_{d,O}$, $k_{d,C}$) of microorganisms, in addition to parameter constraint 7, which conditions the model parameters in a way that the rate of change in the microbial states ($k_{r,O}$,

$k_{r,C}$, $k_{d,O}$, $k_{d,C}$) will be faster than the maximum growth rate ($\mu_{max,O}$; $\mu_{max,C}$) (Blagodatskaya and Kuzyakov, 2013; Konopka, 1999; Salazar et al., 2018). A resultant shift to higher values in the distribution of the reactivation rate constant of the two functional groups ($k_{r,O}$, $k_{r,C}$) due to these constraints was observed (Fig. 3). There was a slight shift to higher values in the distribution of $k_{d,C}$ too when only parameter constraints were applied; however, this shift reverted when process constraints were applied. Cb MCMC also found that the reactivation rate constant for copiotrophs ($k_{r,C}$) is higher than oligotrophs ($k_{r,O}$), indicating that under favorable conditions copiotrophs can become active faster than oligotrophs. This result aligns with the more stable nature of oligotrophs compared to copiotrophs, which grow faster with a shorter life expectancy.

Certain parameters, such as the reduction factor in the dormant state (β_i), could not be improved, due to a lack of information regarding parameter intercorrelations, as shown in the corresponding parameter distributions. Only process constraints slightly shifted the β_C towards lower values. The parameter β_i represents the reduction factor in the maintenance requirements of microorganisms when they are in a dormant state. More experimental data to set up additional constraints regarding the dormant fractions of microorganisms in the rhizosphere is needed to discern specific patterns (Hungate et al., 2015; Metze et al., 2023).

Overall, the application of cb MCMC with the defined parameter and process constraints reduced the parameter space significantly and estimated the patterns for most of the microbial functional group-related parameters. Parameter constraints alone were insufficient to estimate the correct pattern for every parameter. Process constraints from experimental evidence were crucial for estimating a corrector parameter distribution. For some parameters, defining more constraints in light of additional experimental evidence would enable to further confine the parameter space.

3.1.3. Trade-offs

Parameter constraints 1 and 2 successfully induced a trade-off between substrate affinity ($k_{i,L}$) and maximum growth rate ($\mu_{max,i}$) for two microbial functional groups. The incorporation of process constraints, grounded in experimental knowledge, narrowed down the parameter space and clarified the functional classification (Fig. 4A).

Trade-off between the maintenance rate ($m_{max,i}$) and growth yield (Y_i) was reflected in the model through the parameter constraints 3 and 8 (Table 5). Process constraints resulted in a shift in the distribution of oligotrophic parameters by constraining growth yield to higher values and maintenance rate to lower values. In the parameters of the copiotrophs, a slight shift towards lower maintenance rates was observed (Fig. 4B).

Another microbial trade-off between growth yield (Y_i) and the threshold substrate concentration for the activation of microorganisms ($C_{thres,i}$) was captured by the model through parameter constraints 4 and 8. Process constraints further shifted the distributions of $C_{thres,i}$ to higher values for both groups (Fig. 4C).

Similarly, parameter constraints 2 and 3 facilitated the trade-off between substrate affinity ($k_{i,S}$) and maintenance rate ($m_{max,i}$). The trade-off between substrate affinity and maintenance rate was accentuated in these functional groups when process constraints were applied, aligning with predictions from ecological theory (Fig. 4D).

As a result of cb MCMC, ecological trade-offs between oligotrophs and copiotrophs are well-reflected in the model's parameterization. While parameter constraints contribute to classify the two microbial groups according to their functions by correlating microbial traits through trade-offs, process constraints further emphasize this distinction. In this regard, process constraints are crucial for achieving more specific patterns in the parameter distributions based on experimental evidence, enhancing the model's ability to accurately reflect microbial physiology.

3.2. Simulation results based on conditioned model parameter sets

3.2.1. Concentration profiles

Accumulation of HMW-OC near the root was observed during the first 9 d of root growth, due to rhizodeposition (Fig. 5A). Subsequently, after 15 d from the initiation of rhizodeposition, a nearly homogeneous distribution of HMW-OC was observed, with concentrations ranging between 6 and 15 $\frac{mg}{cm^3}$. Thereafter, no significant changes were noted in the concentration profiles of HMW-OC, attributed to reaching equilibrium.

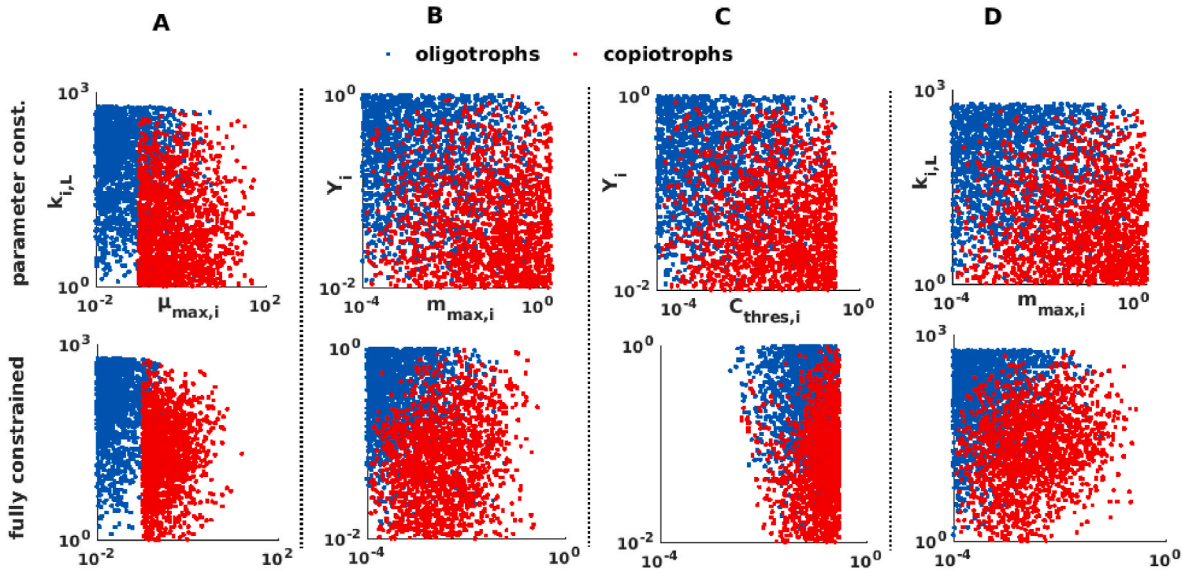

Fig. 4. Scatter plots of the parameters that represent microbial traits which correlate with each other via trade-offs. Resulting parameter distributions are plotted after only applying parameter constraints on top and after applying process constraints on bottom. Blue dots represent the parameter values for oligotrophs while red dots stand for the parameter value for copiotrophs. A) Growth rate ($\mu_{max,i}$) versus substrate affinity ($k_{i,L}$) B) Maintenance yield (Y_i) versus maintenance rate ($m_{max,i}$) C) Maintenance yield (Y_i) versus threshold concentration for reactivation ($C_{thres,i}$) D) Substrate affinity ($k_{i,L}$) versus maintenance rate of microorganisms ($m_{max,i}$). (For interpretation of the references to colour in this figure legend, the reader is referred to the Web version of this article.)

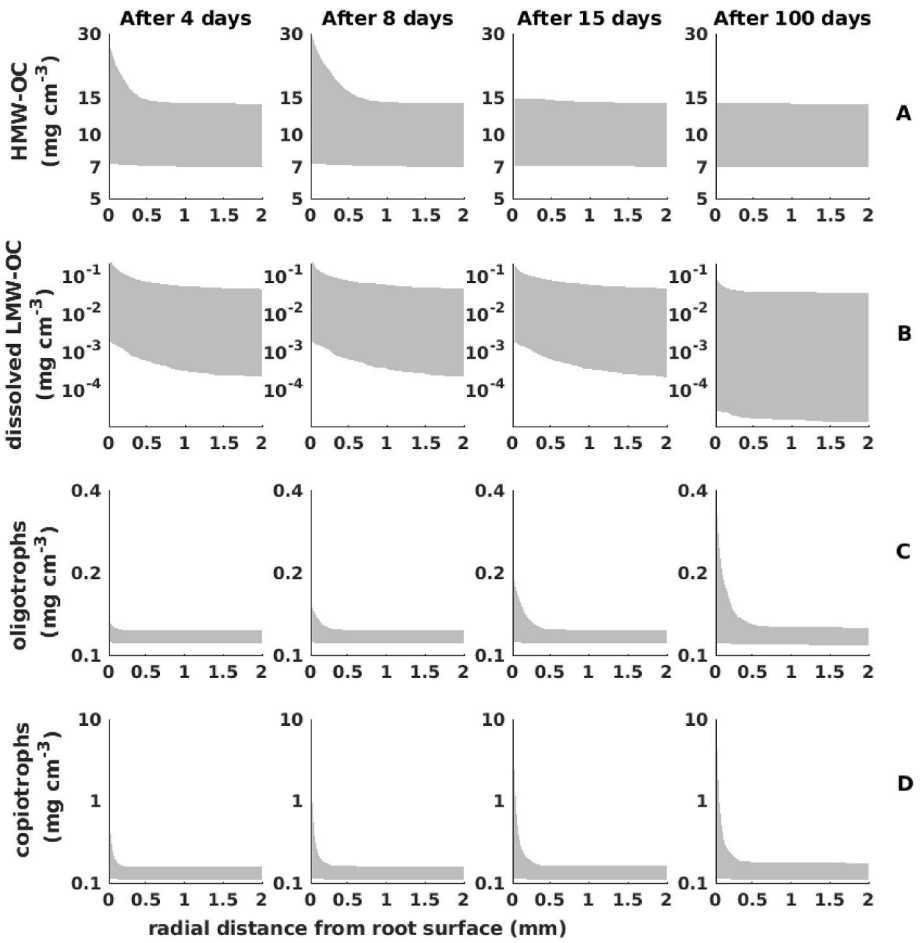

Fig. 5. Concentration profiles of organic carbon and microbial biomass (in log scale) between 0 and 2 mm away from the root surface (no significant change was observed beyond this distance) at 4 days, 8 days, 15 days, and 100 days after root starts to grow and release carbon. From top to bottom: A) High-molecular-weight organic C compounds, B) dissolved low-molecular-weight organic C compounds, C) oligotrophic biomass, D) copiotrophic biomass. Prediction bands for simulated outputs are depicted in grey (95%) for the fully constrained parameter sets.

The concentration of dissolved LMW-OC decreased with increasing distance from the root surface, influenced by the rhizodeposition effect of LMW-OC near the root surface (Fig. 5B). Simulated dissolved LMW-OC concentrations reached up to 0.2 $\frac{mg}{cm^3}$ at the root surface during the initial 15 d of rhizodeposition. Thereafter dissolved LMW-OC at the root surface decreased up to threefold due to microbial uptake. Even after 100 d of root growth, a detectable rhizosphere effect in dissolved LMW-OC persisted. The sustained dissolved LMW-OC gradients after the cessation of root exudation resulted from ongoing root water uptake and the convective transport of dissolved LMW-OC from the soil to the root surface as well as the organic C input from the root to the soil first 15 d. The contribution of each parameter to the persistence of the rhizosphere effect in LMW-OC was analyzed with performing sensitivity analysis in section 3.3.1.

Rhizodeposition had a more pronounced effect on copiotrophic biomass compared to oligotrophic biomass in the first 15 d (Fig. 5C and D). However, spatial patterns of microbial abundance were observed in both groups. Very close to the root surface (0–0.2 mm), both groups exhibited a steep concentration profile.

The simulation periods were extended to 300 d to observe the persistence in the spatial gradients of microbial functional groups. Despite a slowdown in the increase of microbial biomass over time, the spatial gradients of microbial biomass could still be observed after 300 d (Fig. 6). Microorganisms did not rapidly die off when the root stopped releasing C due to their dormancy strategy. This dormancy strategy helped microorganisms survive for an extended period and prevented rapid consumption of the substrate, allowing active microorganisms to grow for a longer period due to the prolonged availability of the substrate.

The proportion of active biomass was highest near the root at the end of rhizodeposition period. While most microorganisms near the root surface were in an active state, the proportion of active biomass was less than 5 percent at 0.6 mm from the root surface after 15 days of growth. The proportion of active copiotrophic biomass decreased to less than 3 percent after 100 days, close to the root surface (<0.6 mm) and decreased further afterwards (Fig. 6D).

On the other hand, oligotrophs remained more active near the root than copiotrophs after 100 days. The proportion of active oligotrophic biomass was less than 3 percent in the soil around the root after 300 days. Spatial gradients of the active biomass persisted longer for oligotrophs than for copiotrophs (Fig. 6C), consistent with the nature of oligotrophs, which change their metabolic states more slowly than copiotrophs, but can stay active in less favorable conditions, as stated in the parametrization section.

3.2.2. *Dynamics of microorganisms and carbon in rhizosphere and bulk soil*

As a result of cb MCMC method, the concentration of HMW-OC in the rhizosphere and bulk soil lies within the range of 7–14 $mg\ cm^{-3}$, following a 1 $mg\ cm^{-3}$ increase in the upper bound of the prediction band for the rhizosphere on the 9th day of rhizodeposition (Fig. 7). After 100 days of root growth, no significant difference was observed between the concentrations of HMW-OC in the rhizosphere and bulk soil

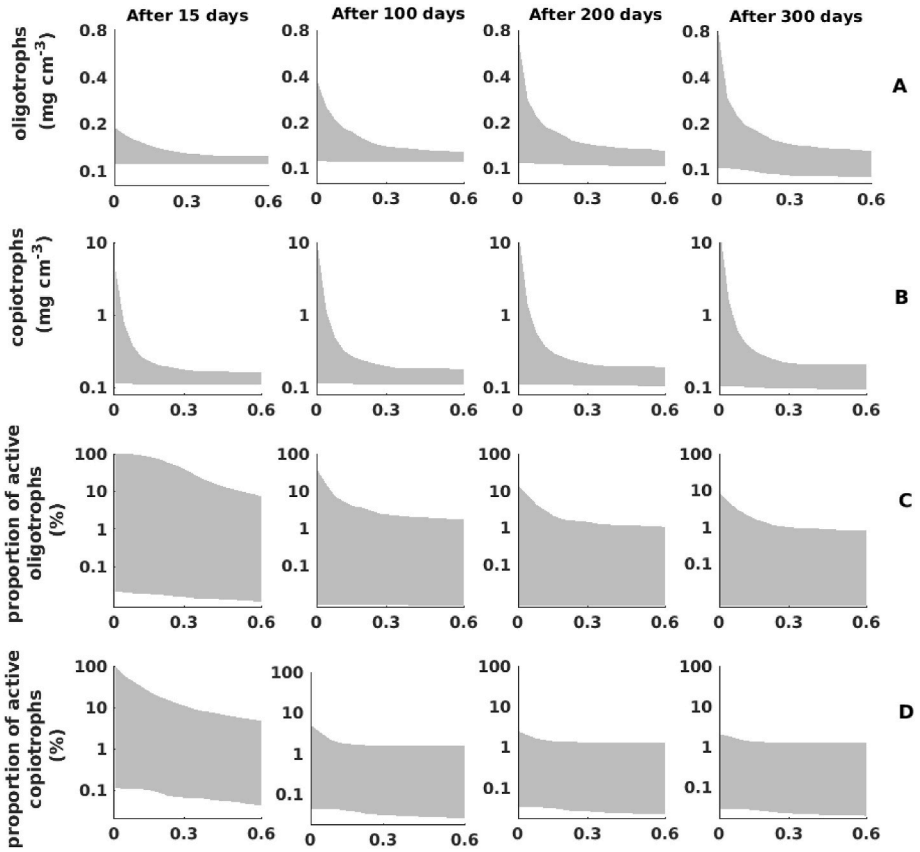

Fig. 6. Concentration profiles of microbial biomass and proportion of active microbial biomass of two functional groups (in log scale) between 0 and 0.6 mm away from the root surface (no significant change was observed beyond this distance) at 15 days, 100 days, 200 days, and 300 days after root starts to grow and release carbon. From top to bottom: A) Oligotrophs, B) copiotrophs, C) proportion of active oligotrophic biomass, D) proportion of active copiotrophic biomass. Prediction bands for simulated outputs are depicted in grey (95%) for the fully constrained parameter sets.

(Fig. 7A).

Dissolved LMW-OC reached its peak in the rhizosphere on the 15th day of root growth. The substantial decrease in dissolved LMW-OC concentration after 15 days, due to ending rhizodeposition, resulted in a decrease of microbial growth, showing up as sharp decline in the proportion of active microbial biomass in the rhizosphere (Fig. 7B–F).

On the 9th day of root growth, the peak of active oligotrophic biomass originates from the ending HMW-OC input from the root. This is so, because oligotrophs play a significant role in the breakdown of HMW-OC (Fig. 7E and F).

Rhizodeposition had a more pronounced effect on total copiotrophs than on oligotrophs, as seen in Fig. 7 (Fig. 7C and D). However, it had a more pronounced effect on active oligotrophic biomass than on active copiotrophic biomass. After 100 days, while copiotrophic biomass was higher than oligotrophic biomass in the rhizosphere, the proportion of active microbial biomass remained higher for oligotrophs than copiotrophs (Fig. 7E and F). After 20 days, the proportion of active biomass to the total biomass in the rhizosphere was less than 7% and 3% for oligotrophs and copiotrophs, respectively. In the bulk soil, the proportion of active microbial biomass did not differ significantly between the two microbial groups; it was below 1.6% (Fig. 7E and F).

3.3. Sensitivity analysis

3.3.1. The long-term effect of rhizodeposition, diffusion and water flux on OC and microbial biomass

Persistence in the spatial patterns of microorganisms was examined by dividing the parameter sets into eight groups based on three key parameters: rate of rhizodeposition, water flux, and diffusion coefficient of dissolved LMW-OC. These parameters are expected to influence the long-lasting spatial gradient of microorganisms and dissolved LMW-OC.

A prolonged rhizosphere effect (after 100 days) on dissolved LMW-OC was observed under conditions of high rhizodeposition, low diffusion, and high water flux (Fig. 8A). The stronger rhizosphere effect observed under low water flux at day 15 was likely due to the contribution of other parameters (e.g., related to microbial uptake or dormancy) influencing the concentration differences. The enduring rhizosphere effect on the microbial functional groups was evident under conditions of high rhizodeposition (Fig. 8B and C), with copiotrophic biomass near the root surpassing that of oligotrophic biomass. Conversely, under conditions of low rhizodeposition, the concentration difference between the root surface and bulk soil was similar and very low for both oligotrophs and copiotrophs after rhizodeposition event.

The diffusion coefficient of dissolved LMW-OC emerged as the second most influential parameter in sustaining the rhizosphere effect (Fig. 8). In scenarios with low diffusion coefficients, a higher gradient of microbial biomass was observed over 300 days. Microbial biomass exhibited steeper concentration profiles over 300 days under conditions of high water flux, facilitating substrate availability near the root (Fig. 8B and C). Despite rhizodeposition ceasing, spatial patterns of both functional groups persisted for 300 days, with the highest contribution from the rhizodeposition rate, indicating the legacy effect of rhizodeposition on microorganisms.

3.3.2. The effect of rhizosphere extent on OC and microbial biomass

The impact of rhizosphere extent on the concentrations of organic C and microbial functional groups was assessed by varying it between 0.5 mm and 2 mm.

HMW-OC did not exhibit significant differences after 20 days for varying rhizosphere diameters, nor did they significantly affect

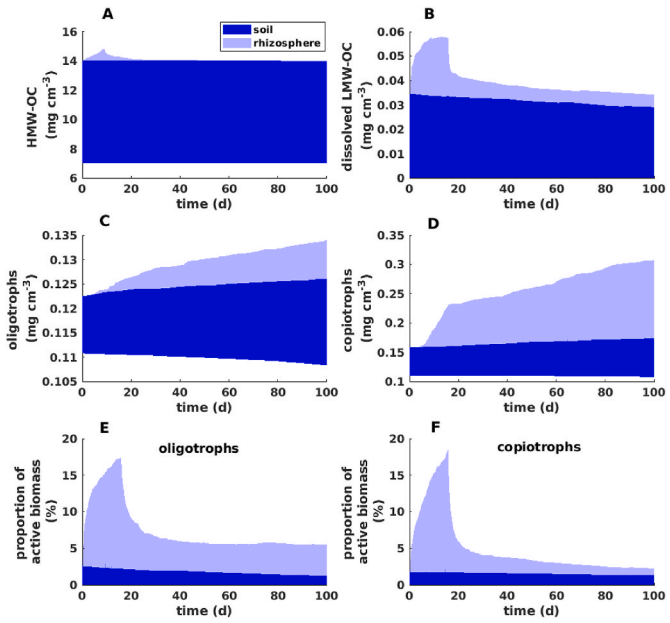

Fig. 7. Temporal changes in A) high-molecular-weight organic C compounds, B) dissolved low-molecular-weight organic C compounds, C) oligotrophic biomass, D) copiotrophic biomass, E) proportion of oligotrophic active biomass to total oligotrophic biomass, and F) proportion of copiotrophic active biomass to total copiotrophic biomass for 100 days, averaged over: 0–2 mm away from the root surface for the rhizosphere, and further away than 2 mm for the bulk soil. The 95% confidence interval for the concentration values in soil (including rhizosphere and bulk soil) is depicted by the dark blue area, while the 95% confidence interval for the concentration values in rhizosphere is represented by the light blue region. (For interpretation of the references to colour in this figure legend, the reader is referred to the Web version of this article.)

dissolved LMW-OC concentrations. However, we observed nearly a two-fold difference in peak concentrations within the first 20 days (Fig. 9A–B). The difference in microorganisms' concentrations as a function of rhizosphere diameter increased gradually over time (Fig. 9C–D). Specifically, the difference of oligotroph concentrations as a function of rhizosphere diameter was up to two-fold (Fig. 9C), whereas for copiotrophs it was approximately up to 1.5-fold (Fig. 9D).

Therefore, rhizosphere extent significantly impacts the concentration of organic C in the rhizosphere during rhizodeposition events, while microbial biomass remains relatively unchanged by varying rhizosphere extent during these events. Conversely, there is no significant impact of rhizosphere extent on organic C after root cessation, unlike microbial biomass, which can significantly change with varying rhizosphere extent.

4. Discussion

Robust predictions of microbial responses to substrate input in the rhizosphere can be achieved with process-based models that parameterize microbial life history strategies based on functional microbial traits and their relationships but are currently limited to individual bacterial strains isolated from rhizosphere soils where a sequenced genome is available (Marschmann et al., 2024). Modeling spatiotemporal patterns of microorganisms and C turnover in the rhizosphere remains thus challenging but is highly relevant to improve the understanding of root-soil interactions and C stabilization mechanisms. While it is still under debate which microbe-based ecological strategies are best suited for predicting the response of microbial communities to environmental changes (Treseder, 2023), there is robust experimental evidence on a bimodal life history strategy that distinguishes between copiotrophs and oligotrophs in the rhizosphere (Ling et al., 2022; López et al., 2023). We therefore integrated a trait-based approach to reflect copiotrophs and oligotrophs in the process-based rhizosphere model TraiRhizo. Model simulations with TraiRhizo enabled to analyse the impact of rhizodeposition on spatiotemporal patterns of microorganisms with distinct responses to varying substrate supply and the associated decomposition and stabilization of organic C in the rhizosphere.

4.1. Prospects and limits of constraint-based parameter sampling for predicting rhizosphere processes

Constraint-based model conditioning with cb MCMC leveraged published experimental evidence and theory to constrain the parameter space of the TraiRhizo model. Parameter constraints limit the parameter space by specifying valid parameter bounds and relationships between parameters. Process constraints limit the parameter space by ensuring that simulated spatiotemporal patterns of microbial biomass and organic C in the rhizosphere and bulk soil are in accordance with experimentally observed patterns. Typically, using a single experimental dataset for model calibration often limits the transferability of the model parameterization to other soil and situations (Scott et al., 1995; Sung et al., 2006; Zelenev et al., 2006). However, by employing cb MCMC, we can holistically integrate informative data from many studies to formulate the constraints. While the predictions are uncertain, cb MCMC provides parameter spaces that allow for robust forecasts and scenario simulations.

The cb MCMC approach is valuable for narrowing down the parameter space by specifying valid parameter bounds and relationships between parameters. It can also be combined with Bayesian calibration to specific experiments to further constrain the parameter space and reduce the uncertainty of model predictions for soil-plant systems. This could be achieved by formulating a combined likelihood function, which would replace the current likelihood function used in the cb MCMC algorithm. By integrating these two approaches, we can enhance the accuracy and reliability of model predictions for specific soil-plant systems (Zamora-Sillero et al., 2011).

4.2. Insights from modeling on spatiotemporal patterns of microbial succession and SOM cycling in the rhizosphere

The model predictions reveal the significant impact of rhizodeposition on the distribution of organic C, microbial biomass, and the proportion of microbial functional groups in the rhizosphere. Rhizodeposition had a more pronounced effect on copiotrophs than oligotrophs, resulting in the dominance of copiotrophs near the root surface where C inputs are high. This outcome aligns with experimental studies showing that bacterial diversity diminishes with increased substrate availability (Ling et al., 2022). However, an opposite effect of rhizodeposition was observed on the active fraction of microbial functional groups. The proportion of active microbial biomass in the rhizosphere remained higher for oligotrophs than for copiotrophs, due to the lower threshold substrate concentration required for the activation of oligotrophs ($C_{thres,O}$). Since oligotrophs play an active role in degrading HMW-OC to LMW-OC, this mechanism led to sustain dissolved LMW-OC, a directly available substrate for microbes, up to 300 days (until the end of simulations) in the rhizosphere.

Another interesting mechanism captured by our model was the steady increase after the rhizodeposition period in the total microbial biomass (active + dormant microbial biomass) up to 300 days in the rhizosphere. This was explained by the dormancy strategy of microorganisms. Most microorganisms transitioned to a dormant metabolic state immediately after rhizodeposition ceased. This dormancy strategy prevents microorganisms from dying off quickly and prevents rapid consumption of the substrate, allowing active microorganisms to grow for an extended period due to the prolonged availability of the substrate.

Additionally, we observed steep gradients in the abundance of two microbial groups within 0–0.2 mm from the root surface especially

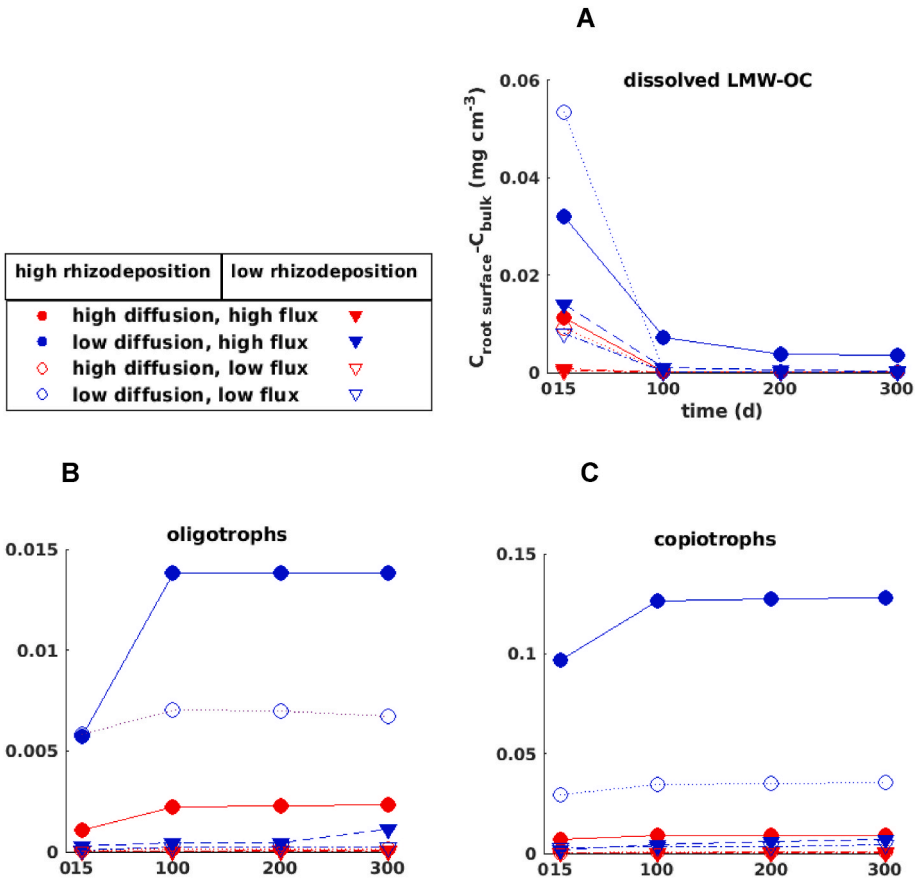

Fig. 8. Concentration differences between root surface and bulk soil for A) dissolved low-molecular-weight organic C compounds (dissolved LMW-OC), B) oligotrophs, and C) copiotrophs at 15 days, 100 days, 200 days, and 300 days after root initiation. Parameter sets are categorized based on the rate of rhizodeposition, water flux, and diffusion coefficient of dissolved low-molecular-weight organic C compounds.

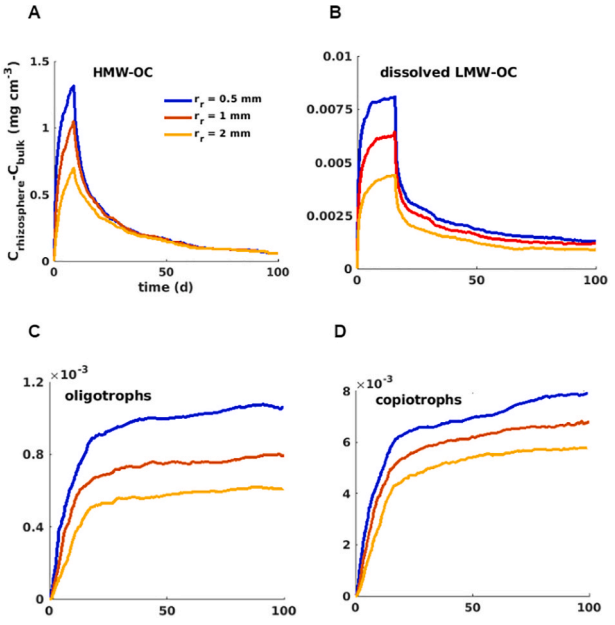

Fig. 9. Temporal dynamics of concentration differences between rhizosphere and bulk soil for A) high-molecular-weight organic C compounds (HMW-OC), B) dissolved low-molecular-weight organic C compounds (dissolved LMW-OC), C) oligotrophs, and D) copiotrophs for three different rhizosphere extent.

under high rhizodeposition conditions, which highlights the importance of resolving soil properties and states at sub-millimeter resolution. The conditioning and the robust quantification of microbial C utilization in the rhizosphere would thus benefit from leveraging spatially resolved soil sampling imaging methods around individual roots.

4.3. *Impact of rhizosphere extent on concentration differences*

In general, experimental investigators have equated the rhizosphere with the soil adhering after physically shaking the root (Chen et al., 2015; Yang et al., 2013). In contrast to this somewhat heuristic view, mathematical modelers have employed different definitions of the rhizosphere (Darrah, 1991; Landl et al., 2021a; Raynaud, 2010). Unfortunately, there is currently no standard definition agreed upon between modelers and experimenters. In this study, we made a pragmatic choice for the rhizosphere extent of 2 mm to align with the experiments used in defining the constraints. This value was also used to differentiate between rhizosphere soil and bulk soil when calculating the dynamics of C pools and microbial biomass in Fig. 7. Consequently, we conducted an analysis with varying rhizosphere extents to understand the effect of rhizosphere extent on the temporal patterns of C pools and microbial biomass.

Our analysis indicated that variations in rhizosphere extent, ranging from 0.5 to 2 mm, have significant effects on C pools, particularly during periods of rhizodeposition and significant effects on the microbial C pools after the rhizodeposition. This highlights the importance of incorporating the spatial variation of concentrations into rhizosphere modeling to ensure accurate predictions of nutrient dynamics. Thus, it is important to consistently define the soil- and plant-specific spatial

extent of the rhizosphere for simulations and experiments on root zone dynamics.

4.4. Legacy effects of rhizodeposition on microorganisms

Our simulations revealed the persistence of spatial patterns of microbial functional groups even after the cessation of root exudation. This legacy effect of rhizodeposition on microbial communities underscores the long-term impact of plant roots on soil microbial dynamics in line with experimental evidence (Hannula et al., 2021; Schmid et al., 2021). The legacy effect was observable for 300 days under high rhizodeposition conditions. Interestingly, oligotrophs exhibited a longer-lasting legacy effect compared to copiotrophs, consistent with their ability to maintain active states for extended periods under nutrient-poor conditions. This could positively affect subsequent root development since oligotrophs play a crucial role in nutrient cycling through mineralization, providing nutrients directly available to plant roots and supporting growth (Bledsoe et al., 2020; Villalobos-Vega et al., 2011). Additionally, oligotrophs' high growth yield traits might reduce microbial-plant nutrient competition due to less nutrient uptake by microorganisms during the plant's growing stage, facilitating nutrient uptake by plant roots (Fierer et al., 2007; Zelenev et al., 2006). However, our model does not address the impact of rhizodeposition legacy on the subsequent root growth. This could be investigated by using coupled trait-based rhizosphere models with root structural models that account for nutrient cycling at the root system scale, as discussed in section 4.5 (Schnepf et al., 2018). Enhancing our knowledge at the plant scale could enable the design of root architectures that increase sustainability and yield (Nannipieri et al., 2023).

4.5. Conclusions and outlook

The applied constraint-based model conditioning closely links recent rhizosphere modelling approaches with the existing experimental findings. Parameter and process constraints were set based on ecological theory and a comprehensive literature analysis to ensure solid grounding. This workflow provides a systematic approach to integrate informative data from upcoming elaborate experiments, which are needed to increase the currently limited empirical evidence in rhizosphere ecology. Our findings demonstrate that rhizodeposition significantly influences the spatiotemporal distribution of microbial functional groups, with oligotrophs showing a longer-lasting legacy effect compared to copiotrophs. This could have important implications for nutrient cycling and subsequent root development due to the role of microbial functional groups in soil health and plant growth.

Further research should focus on the effects of varying soil conditions, such as soil moisture and pH, on microbial community dynamics in the rhizosphere. Combining model simulations with empirical data from field studies will provide a more comprehensive understanding of these interactions. Additionally, investigating the impact of rhizodeposition legacy on subsequent root growth through coupled trait-based rhizosphere models with root structural models will be crucial for designing sustainable root architectures.

Our future goal is to implement a three-dimensional coupling of the TraiRhizo model with the structural-functional plant model CPlantBox (Giraud et al., 2023). This integration will allow for a deeper understanding of plant-microbe interactions, ecosystem functioning, and the feedbacks between root growth and rhizosphere processes.

CRediT authorship contribution statement

Ahmet Kürşad Sırcan: Writing – original draft, Visualization, Software, Methodology, Investigation, Formal analysis. **Thilo Streck:** Writing – review & editing, Supervision, Methodology, Funding acquisition, Conceptualization. **Andrea Schnepf:** Writing – review & editing, Supervision, Methodology, Funding acquisition, Conceptualization. **Mona Giraud:** Writing – review & editing, Methodology. **Adrian Lattacher:** Writing – review & editing. **Ellen Kandeler:** Writing – review & editing, Funding acquisition. **Christian Poll:** Writing – review & editing, Funding acquisition. **Holger Pagel:** Writing – review & editing, Supervision, Software, Methodology, Funding acquisition, Conceptualization.

Declaration of competing interest

The authors declare that they have no known competing financial interests or personal relationships that could have appeared to influence the work reported in this paper.

Acknowledgments

The authors acknowledge funding by the German Federal Ministry of Education and Research (BMBF) in the framework of the funding measure "Plant roots and soil ecosystems, significance of the rhizosphere for the bio-economy" (Rhizo4Bio), subproject CROP (FKZ 031B0909). Further funding is appreciated from the German Research Foundation (DFG) within the priority program 2322 "Soil Systems" (STR 481/12-1) and under Germany's Excellence Strategy (EXC 2070–390732324).

Appendix A. Supplementary data

Supplementary data to this article can be found online at https://doi.org/10.1016/j.soilbio.2024.109698.

References

Blagodatskaya, E., Kuzyakov, Y., 2013. Active microorganisms in soil: critical review of estimation criteria and approaches. Soil Biology and Biochemistry 67, 192–211. https://doi.org/10.1016/j.soilbio.2013.08.024.

Blagodatskaya, E., Littschwager, J., Lauerer, M., Kuzyakov, Y., 2014. Plant traits regulating N capture define microbial competition in the rhizosphere. European Journal of Soil Biology 61, 41–48. https://doi.org/10.1016/j.ejsobi.2014.01.002.

Blagodatskaya, E., Tarkka, M., Knief, C., Koller, R., Peth, S., Schmidt, V., Spielvogel, S., Uteau, D., Weber, M., Razavi, B.S., 2021. Bridging microbial functional traits with localized process rates at soil interfaces. Frontiers in Microbiology 12, 625697. https://doi.org/10.3389/fmicb.2021.625697.

Blagodatskaya, E.V., Blagodatsky, S.A., Anderson, T.H., Kuzyakov, Y., 2009. Contrasting effects of glucose, living roots and maize straw on microbial growth kinetics and substrate availability in soil. European Journal of Soil Science 60 (2), 186–197. https://doi.org/10.1111/j.1365-2389.2008.01103.x.

Blake, G.R., 2008. Particle density. In: Chesworth, W. (Ed.), Encyclopedia of Soil Science. Springer, Netherlands, pp. 504–505. https://doi.org/10.1007/978-1-4020-3995-9_406.

Bledsoe, R.B., Goodwillie, C., Peralta, A.L., 2020. Long-term nutrient enrichment of an oligotroph-dominated wetland increases bacterial diversity in bulk soils and plant rhizospheres. mSphere 5 (3). https://doi.org/10.1128/mSphere.00035-20.

Bonkowski, M., Cheng, W., Griffiths, B.S., Alphei, J., Scheu, S., 2000. Microbial-faunal interactions in the rhizosphere and effects on plant growth. European Journal of Soil Biology 36 (3–4), 135–147. https://doi.org/10.1016/S1164-5563(00)01059-1.

Bulgarelli, D., Schlaeppi, K., Spaepen, S., Van Themaat, E.V.L., Schulze-Lefert, P., 2013. Structure and functions of the bacterial microbiota of plants. Annual Review of Plant Biology 64 (1), 807–838. https://doi.org/10.1146/annurev-arplant-050312-120106.

Chari, N.R., Tumber-Dávila, S.J., Phillips, R.P., Bauerle, T.L., Brunn, M., Hafner, B.D., Klein, T., Obersteiner, S., Reay, M.K., Ullah, S., Taylor, B.N., 2024. *The global root exudate carbon flux* [Preprint]. Ecology. https://doi.org/10.1101/2024.02.01.578470.

Chavez Rodriguez, L., González-Nicolás, A., Ingalls, B., Streck, T., Nowak, W., Xiao, S., Pagel, H., 2022. Optimal design of experiments to improve the characterisation of atrazine degradation pathways in soil. European Journal of Soil Science 73 (1), e13211. https://doi.org/10.1111/ejss.13211.

Chen, Z., Wang, X., Shang, H., 2015. Structure and function of rhizosphere and non-rhizosphere soil microbial community respond differently to elevated ozone in field-planted wheat. Journal of Environmental Sciences 32, 126–134. https://doi.org/10.1016/j.jes.2014.12.018.

Clark, F.E., 1949. Soil microorganisms and plant roots. Advances in Agronomy 1, 241–288. https://doi.org/10.1016/S0065-2113(08)60750-6. Elsevier.

Darrah, P.R., 1991. Models of the rhizosphere: I. Microbial population dynamics around a root releasing soluble and insoluble carbon. Plant and Soil 133 (2), 187–199. https://doi.org/10.1007/BF00009191.

Dupuy, L.X., Silk, W.K., 2016. Mechanisms of early microbial establishment on growing root surfaces. Vadose Zone Journal 15 (2), 1–13. https://doi.org/10.2136/vzj2015.06.0094.

Fang, H., Cheng, S., Lin, E., Yu, G., Niu, S., Wang, Y., Xu, M., Dang, X., Li, L., Wang, L., 2015. Elevated atmospheric carbon dioxide concentration stimulates soil microbial activity and impacts water-extractable organic carbon in an agricultural soil. Biogeochemistry 122 (2–3), 253–267. https://doi.org/10.1007/s10533-014-0039-2.

Fatichi, S., Manzoni, S., Or, D., Paschalis, A., 2019. A mechanistic model of microbially mediated soil biogeochemical processes: a reality check. Global Biogeochemical Cycles 33 (6), 620–648. https://doi.org/10.1029/2018GB006077.

Faybishenko, B., Molz, F., 2013. Nonlinear rhizosphere dynamics yields synchronized oscillations of microbial populations, carbon and oxygen concentrations, induced by root exudation. Procedia Environmental Sciences 19, 369–378. https://doi.org/10.1016/j.proenv.2013.06.042.

Fierer, N., Bradford, M.A., Jackson, R.B., 2007. Toward an ecological classification of soil bacteria. Ecology 88 (6), 1354–1364. https://doi.org/10.1890/05-1839.

Fierer, N., Lauber, C.L., Ramirez, K.S., Zaneveld, J., Bradford, M.A., Knight, R., 2012. Comparative metagenomic, phylogenetic and physiological analyses of soil microbial communities across nitrogen gradients. The ISME Journal 6 (5), 1007–1017. https://doi.org/10.1038/ismej.2011.159.

Giraud, M., Gall, S.L., Harings, M., Javaux, M., Leitner, D., Meunier, F., Rothfuss, Y., Van Dusschoten, D., Vanderborght, J., Vereecken, H., Lobet, G., Schnepf, A., 2023. CPlantBox: a fully coupled modelling platform for the water and carbon fluxes in the soil–plant–atmosphere continuum. Silico Plants 5 (2), diad009. https://doi.org/10.1093/insilicoplants/diad009.

Hannula, S.E., Heinen, R., Huberty, M., Steinauer, K., De Long, J.R., Jongen, R., Bezemer, T.M., 2021. Persistence of plant-mediated microbial soil legacy effects in soil and inside roots. Nature Communications 12 (1), 5686. https://doi.org/10.1038/s41467-021-25971-z.

Hartmann, A., Schmid, M., Tuinen, D.V., Berg, G., 2009. Plant-driven selection of microbes. Plant and Soil 321 (1–2), 235–257. https://doi.org/10.1007/s11104-008-9814-y.

Hellweger, F.L., Clegg, R.J., Clark, J.R., Plugge, C.M., Kreft, J.-U., 2016. Advancing microbial sciences by individual-based modelling. Nature Reviews Microbiology 14 (7), 461–471. https://doi.org/10.1038/nrmicro.2016.62.

Hinsinger, P., Bengough, A.G., Vetterlein, D., Young, I.M., 2009. Rhizosphere: biophysics, biogeochemistry and ecological relevance. Plant and Soil 321 (1–2), 117–152. https://doi.org/10.1007/s11104-008-9885-9.

Ho, A., Lonardo, D.P.D., Bodelier, P.L.E., 2017. Revisiting life strategy concepts in environmental microbial ecology. FEMS Microbiology Ecology fix006. https://doi.org/10.1093/femsec/fix006.

Hu, L., Robert, C.A.M., Cadot, S., Zhang, X., Ye, M., Li, B., Manzo, D., Chervet, N., Steinger, T., Van Der Heijden, M.G.A., Schlaeppi, K., Erb, M., 2018. Root exudate metabolites drive plant-soil feedbacks on growth and defense by shaping the rhizosphere microbiota. Nature Communications 9 (1), 2738. https://doi.org/10.1038/s41467-018-05122-7.

Hungate, B.A., Mau, R.L., Schwartz, E., Caporaso, J.G., Dijkstra, P., Van Gestel, N., Koch, B.J., Liu, C.M., McHugh, T.A., Marks, J.C., Morrissey, E.M., Price, L.B., 2015. Quantitative microbial ecology through stable isotope probing. Applied and Environmental Microbiology 81 (21), 7570–7581. https://doi.org/10.1128/AEM.02280-15.

Jagadamma, S., Mayes, M.A., Phillips, J.R., 2012. Selective sorption of dissolved organic carbon compounds by temperate soils. PLoS One 7 (11). doi:10.1371/journal.pone.0050434.

Jagadamma, S., Mayes, M.A., Zinn, Y.L., Gísladóttir, G., Russell, A.E., 2014. Sorption of organic carbon compounds to the fine fraction of surface and subsurface soils. Geoderma 213, 79–86. https://doi.org/10.1016/j.geoderma.2013.07.030.

Jat, H.S., Datta, A., Choudhary, M., Sharma, P.C., Dixit, B., Jat, M.L., 2021. Soil enzymes activity: effect of climate smart agriculture on rhizosphere and bulk soil under cereal based systems of north-west India. European Journal of Soil Biology 103, 103292. https://doi.org/10.1016/j.ejsobi.2021.103292.

Jin, J., Krohn, C., Franks, A.E., Wang, X., Wood, J.L., Petrovski, S., McCaskill, M., Batinovic, S., Xie, Z., Tang, C., 2022. Elevated atmospheric CO2 alters the microbial community composition and metabolic potential to mineralize organic phosphorus in the rhizosphere of wheat. Microbiome 10 (1), 12. https://doi.org/10.1186/s40168-021-01203-w.

König, S., Vogel, H.-J., Harms, H., Worrich, A., 2020. Physical, chemical and biological effects on soil bacterial dynamics in microscale models. Frontiers in Ecology and Evolution 8, 53. https://doi.org/10.3389/fevo.2020.00053.

Konopka, A., 1999. Theoretical analysis of the starvation response under substrate pulses. Microbial Ecology 38 (4), 321–329. https://doi.org/10.1007/s002489900178.

Kothawala, D.N., Moore, T.R., Hendershot, W.H., 2009. Soil properties controlling the adsorption of dissolved organic carbon to mineral soils. Soil Science Society of America Journal 73 (6), 1831–1842. https://doi.org/10.2136/sssaj2008.0254.

Kravchenko, L.V., Strigul', N.S., Shvytov, I.A., 2004. Mathematical simulation of the dynamics of interacting populations of rhizosphere microorganisms. Microbiology 73 (2), 189–195. https://doi.org/10.1023/B:MICI.0000023988.11064.43.

Kuppe, C.W., Schnepf, A., Von Lieres, E., Watt, M., Postma, J.A., 2022. Rhizosphere models: their concepts and application to plant-soil ecosystems. Plant and Soil 474 (1–2), 17–55. https://doi.org/10.1007/s11104-021-05201-7.

Kuzyakov, Y., Blagodatskaya, E., 2015. Microbial hotspots and hot moments in soil: concept & review. Soil Biology and Biochemistry 83, 184–199. https://doi.org/10.1016/j.soilbio.2015.01.025.

Kuzyakov, Y., Razavi, B.S., 2019. Rhizosphere size and shape: temporal dynamics and spatial stationarity. Soil Biology and Biochemistry 135, 343–360. https://doi.org/10.1016/j.soilbio.2019.05.011.

Landl, M., Phalempin, M., Schlüter, S., Vetterlein, D., Vanderborght, J., Kroener, E., Schnepf, A., 2021a. Modeling the impact of rhizosphere bulk density and mucilage gradients on root water uptake. Frontiers in Agronomy 3, 622367. https://doi.org/10.3389/fagro.2021.622367.

Landl, M., Haupenthal, A., Leitner, D., Kroener, E., Vetterlein, D., Bol, R., Vereecken, H., Vanderborght, J., Schnepf, A., 2021b. Simulating rhizodeposition patterns around growing and exuding root systems. Silico Plants 3 (2), diab028. https://doi.org/10.1093/insilicoplants/diab028.

Lauro, F.M., McDougald, D., Thomas, T., Williams, T.J., Egan, S., Rice, S., DeMaere, M.Z., Ting, L., Ertan, H., Johnson, J., Ferriera, S., Lapidus, A., Anderson, I., Kyrpides, N., Munk, A.C., Detter, C., Han, C.S., Brown, M.V., Robb, F.T., et al., 2009. The genomic basis of trophic strategy in marine bacteria. Proceedings of the National Academy of Sciences 106 (37), 15527–15533. https://doi.org/10.1073/pnas.0903507106.

Lehmann, J., Hansel, C.M., Kaiser, C., Kleber, M., Maher, K., Manzoni, S., Nunan, N., Reichstein, M., Schimel, J.P., Torn, M.S., Wieder, W.R., Kögel-Knabner, I., 2020. Persistence of soil organic carbon caused by functional complexity. Nature Geoscience 13 (8), 529–534. https://doi.org/10.1038/s41561-020-0612-3.

Lehmann, J., Kleber, M., 2015. The contentious nature of soil organic matter. Nature 528 (7580), 60–68. https://doi.org/10.1038/nature16069.

Li, X., Deng, Y., Li, Q., Lu, C., Wang, J., Zhang, H., Zhu, J., Zhou, J., He, Z., 2013. Shifts of functional gene representation in wheat rhizosphere microbial communities under elevated ozone. The ISME Journal 7 (3), 660–671. https://doi.org/10.1038/ismej.2012.120.

Ling, N., Wang, T., Kuzyakov, Y., 2022. Rhizosphere bacteriome structure and functions. Nature Communications 13 (1), 836. https://doi.org/10.1038/s41467-022-28448-9.

Lipson, D.A., 2015. The complex relationship between microbial growth rate and yield and its implications for ecosystem processes. Frontiers in Microbiology 6. https://doi.org/10.3389/fmicb.2015.00615.

López, J.L., Fourie, A., Poppeliers, S.W.M., Pappas, N., Sánchez-Gil, J.J., De Jonge, R., Dutilh, B.E., 2023. Growth rate is a dominant factor predicting the rhizosphere effect. The ISME Journal 17 (9), 1396–1405. https://doi.org/10.1038/s41396-023-01453-6.

Malik, A.A., Martiny, J.B.H., Brodie, E.L., Martiny, A.C., Treseder, K.K., Allison, S.D., 2020. Defining trait-based microbial strategies with consequences for soil carbon cycling under climate change. The ISME Journal 14 (1), 1–9. https://doi.org/10.1038/s41396-019-0510-0.

Marschmann, G.L., Pagel, H., Kügler, P., Streck, T., 2019. Equifinality, sloppiness, and emergent structures of mechanistic soil biogeochemical models. Environmental Modelling & Software 122, 104518. https://doi.org/10.1016/j.envsoft.2019.104518.

Marschmann, G.L., Tang, J., Zhalnina, K., Karaoz, U., Cho, H., Le, B., Pett-Ridge, J., Brodie, E.L., 2024. Predictions of rhizosphere microbiome dynamics with a genome-informed and trait-based energy budget model. Nature Microbiology 9 (2), 421–433. https://doi.org/10.1038/s41564-023-01582-w.

Matthews, A., Pierce, S., Hipperson, H., Raymond, B., 2019. Rhizobacterial community assembly patterns vary between crop species. Frontiers in Microbiology 10, 581. https://doi.org/10.3389/fmicb.2019.00581.

Mayes, M.A., Heal, K.R., Brandt, C.C., Phillips, J.R., Jardine, P.M., 2012. Relation between soil order and sorption of dissolved organic carbon in temperate subsoils. Soil Science Society of America Journal 76 (3), 1027–1037. https://doi.org/10.2136/sssaj2011.0340.

Metze, D., Schnecker, J., Canarini, A., Fuchslueger, L., Koch, B.J., Stone, B.W., Hungate, B.A., Hausmann, B., Schmidt, H., Schaumberger, A., Bahn, M., Kaiser, C., Richter, A., 2023. Microbial growth under drought is confined to distinct taxa and modified by potential future climate conditions. Nature Communications 14 (1), 5895. https://doi.org/10.1038/s41467-023-41524-y.

Millington, R.J., Quirk, J.P., 1961. Permeability of porous solids. Transactions of the Faraday Society 57, 1200. https://doi.org/10.1039/tf9615701200.

Nannipieri, P., Hannula, S.E., Pietramellara, G., Schloter, M., Sizmur, T., Pathan, S.I., 2023. Legacy effects of rhizodeposits on soil microbiomes: a perspective. Soil Biology and Biochemistry 184, 109107. https://doi.org/10.1016/j.soilbio.2023.109107.

Norton, J.M., Firestone, M.K., 1991. Metabolic status of bacteria and fungi in the rhizosphere of ponderosa pine seedlings. Applied and Environmental Microbiology 57 (4), 1161–1167. https://doi.org/10.1128/aem.57.4.1161-1167.1991.

Nuccio, E.E., Starr, E., Karaoz, U., Brodie, E.L., Zhou, J., Tringe, S.G., Malmstrom, R.R., Woyke, T., Banfield, J.F., Firestone, M.K., Pett-Ridge, J., 2020. Niche differentiation is spatially and temporally regulated in the rhizosphere. The ISME Journal 14 (4), 999–1014. https://doi.org/10.1038/s41396-019-0582-x.

Nye, P.H., Marriott, F.H.C., 1969. A theoretical study of the distribution of substances around roots resulting from simultaneous diffusion and mass flow. Plant and Soil 30 (3), 459–472. https://doi.org/10.1007/BF01881971.

Pagel, H., Kriesche, B., Uksa, M., Poll, C., Kandeler, E., Schmidt, V., Streck, T., 2020. Spatial control of carbon dynamics in soil by microbial decomposer communities. Frontiers in Environmental Science 8, 2. https://doi.org/10.3389/fenvs.2020.00002.

Pagel, H., Poll, C., Ingwersen, J., Kandeler, E., Streck, T., 2016. Modeling coupled pesticide degradation and organic matter turnover: from gene abundance to process rates. Soil Biology and Biochemistry 103, 349–364. https://doi.org/10.1016/j.soilbio.2016.09.014.

Papp, K., Hungate, B.A., Schwartz, E., 2020. Glucose triggers strong taxon-specific responses in microbial growth and activity: insights from DNA and RNA qSIP. Ecology 101 (1), e02887. https://doi.org/10.1002/ecy.2887.

Philippot, L., Raaijmakers, J.M., Lemanceau, P., Van Der Putten, W.H., 2013. Going back to the roots: the microbial ecology of the rhizosphere. Nature Reviews Microbiology 11 (11), 789–799. https://doi.org/10.1038/nrmicro3109.

Raynaud, X., 2010. Soil properties are key determinants for the development of exudate gradients in a rhizosphere simulation model. Soil Biology and Biochemistry 42 (2), 210–219. https://doi.org/10.1016/j.soilbio.2009.10.019.

Raynaud, X., Lata, J.-C., Leadley, P.W., 2006. Soil microbial loop and nutrient uptake by plants: a test using a coupled C:N model of plant–microbial interactions. Plant and Soil 287 (1–2), 95–116. https://doi.org/10.1007/s11104-006-9003-9.

Roller, B.R.K., Stoddard, S.F., Schmidt, T.M., 2016. Exploiting rRNA operon copy number to investigate bacterial reproductive strategies. Nature Microbiology 1 (11), 16160. https://doi.org/10.1038/nmicrobiol.2016.160.

Russell, R.S., 1978. Plant root systems: their function and interaction with the soil. Soil Science 125 (4), 272. https://doi.org/10.1097/00010694-197804000-00023.

Salazar, A., Lennon, J.T., Dukes, J.S., 2019. Microbial dormancy improves predictability of soil respiration at the seasonal time scale. Biogeochemistry 144 (1), 103–116. https://doi.org/10.1007/s10533-019-00574-5.

Salazar, A., Sulman, B.N., Dukes, J.S., 2018. Microbial dormancy promotes microbial biomass and respiration across pulses of drying-wetting stress. Soil Biology and Biochemistry 116, 237–244. https://doi.org/10.1016/j.soilbio.2017.10.017.

Schenck Zu Schweinsberg-Mickan, M., Jörgensen, R.G., Müller, T., 2012. Rhizodeposition: its contribution to microbial growth and carbon and nitrogen turnover within the rhizosphere. Journal of Plant Nutrition and Soil Science 175 (5), 750–760. https://doi.org/10.1002/jpln.201100300.

Schmid, M.W., Van Moorsel, S.J., Hahl, T., De Luca, E., De Deyn, G.B., Wagg, C., Niklaus, P.A., Schmid, B., 2021. Effects of plant community history, soil legacy and plant diversity on soil microbial communities. Journal of Ecology 109 (8), 3007–3023. https://doi.org/10.1111/1365-2745.13714.

Schnepf, A., Carminati, A., Ahmed, M.A., Ani, M., Benard, P., Bentz, J., Bonkowski, M., Knott, M., Diehl, D., Duddek, P., Kröner, E., Javaux, M., Landl, M., Lehndorff, E., Lippold, E., Lieu, A., Mueller, C.W., Oburger, E., Otten, W., et al., 2022. Linking rhizosphere processes across scales: opinion. Plant and Soil 478 (1–2), 5–42. https://doi.org/10.1007/s11104-022-05306-7.

Schnepf, A., Leitner, D., Landl, M., Lobet, G., Mai, T.H., Morandage, S., Sheng, C., Zörner, M., Vanderborght, J., Vereecken, H., 2018. CRootBox: a structural–functional modelling framework for root systems. Annals of Botany 121 (5), 1033–1053. https://doi.org/10.1093/aob/mcx221.

Schwarz, K., Reinersmann, T., Heil, J., Marschner, B., Stumpe, B., 2022. Spatio-temporal characterization of microbial heat production on undisturbed soil samples combining infrared thermography and zymography. Geoderma 418, 115821. https://doi.org/10.1016/j.geoderma.2022.115821.

Scott, E.M., Rattray, E.A.S., Prosser, J.I., Killham, K., Glover, L.A., Lynch, J.M., Bazin, M. J., 1995. A mathematical model for dispersal of bacterial inoculants colonizing the wheat rhizosphere. Soil Biology and Biochemistry 27 (10), 1307–1318. https://doi.org/10.1016/0038-0717(95)00050-O.

Stolpovsky, K., Martinez-Lavanchy, P., Heipieper, H.J., Van Cappellen, P., Thullner, M., 2011. Incorporating dormancy in dynamic microbial community models. Ecological Modelling 222 (17), 3092–3102. https://doi.org/10.1016/j.ecolmodel.2011.07.006.

Streck, T., Poletika, N., Jury, W.A., Farmer, W.J., 1995. Description of simazine transport with rate-limited, two-stage, linear and nonlinear sorption. Water Resources Research 31 (4), 811–822. https://doi.org/10.1029/94WR02822.

Strigul, N.S., Kravchenko, L.V., 2006. Mathematical modeling of PGPR inoculation into the rhizosphere. Environmental Modelling & Software 21 (8), 1158–1171. https://doi.org/10.1016/j.envsoft.2005.06.003.

Sung, K., Kim, J., Munster, C.L., Corapcioglu, M.Y., Park, S., Drew, M.C., Chang, Y.Y., 2006. A simple approach to modeling microbial biomass in the rhizosphere. Ecological Modelling 190 (3–4), 277–286. https://doi.org/10.1016/j.ecolmodel.2005.04.020.

Swenson, H., Stadie, N.P., 2019. Langmuir's theory of adsorption: a centennial review. Langmuir 35 (16), 5409–5426. https://doi.org/10.1021/acs.langmuir.9b00154.

Szegedi, K., Vetterlein, D., Nietfeld, H., Jahn, R., Neue, H., 2008. New tool RhizoMath for modeling coupled transport and speciation in the rhizosphere. Vadose Zone Journal 7 (2), 712–720. https://doi.org/10.2136/vzj2007.0064.

Treseder, K.K., 2023. Ecological strategies of microbes: thinking outside the triangle. Journal of Ecology 111 (9), 1832–1843. https://doi.org/10.1111/1365-2745.14115.

Villalobos-Vega, R., Goldstein, G., Haridasan, M., Franco, A.C., Miralles-Wilhelm, F., Scholz, F.G., Bucci, S.J., 2011. Leaf litter manipulations alter soil physicochemical properties and tree growth in a Neotropical savanna. Plant and Soil 346 (1–2), 385–397. https://doi.org/10.1007/s11104-011-0860-5.

Von Jeetze, P.J., Zarebanadkouki, M., Carminati, A., 2020. Spatial heterogeneity enables higher root water uptake in dry soil but protracts water stress after transpiration decline: a numerical study. Water Resources Research 56 (1), e2019WR025501. https://doi.org/10.1029/2019WR025501.

Wieder, W.R., Grandy, A.S., Kallenbach, C.M., Taylor, P.G., Bonan, G.B., 2015. *Representing life in the Earth system with soil microbial functional traits in the MIMICS model* [Preprint]. Biogeosciences. https://doi.org/10.5194/gmdd-8-2011-2015.

Williams, M., Yanai, R.D., 1996. Multi-dimensional sensitivity analysis and ecological implications of a nutrient uptake model. Plant and Soil 180 (2), 311–324. https://doi.org/10.1007/BF00015315.

Xu, Q., Wang, X., Tang, C., 2019. Rhizosphere priming of two near-isogenic wheat lines varying in citrate efflux under different levels of phosphorus supply. Annals of Botany 124 (6), 1033–1042. https://doi.org/10.1093/aob/mcz082.

Yang, Q., Wang, X., Shen, Y., 2013. Comparison of soil microbial community catabolic diversity between rhizosphere and bulk soil induced by tillage or residue retention. Journal of Soil Science and Plant Nutrition. https://doi.org/10.4067/S0718-95162013005000017. *ahead*, 0–0.

Zamora-Sillero, E., Hafner, M., Ibig, A., Stelling, J., Wagner, A., 2011. Efficient characterization of high-dimensional parameter spaces for systems biology. BMC Systems Biology 5 (1), 142. https://doi.org/10.1186/1752-0509-5-142.

Zarebanadkouki, M., Trtik, P., Hayat, F., Carminati, A., Kaestner, A., 2019. Root water uptake and its pathways across the root: quantification at the cellular scale. Scientific Reports 9 (1), 12979. https://doi.org/10.1038/s41598-019-49528-9.

Zarraonaindia, I., Owens, S.M., Weisenhorn, P., West, K., Hampton-Marcell, J., Lax, S., Bokulich, N.A., Mills, D.A., Martin, G., Taghavi, S., Van Der Lelie, D., Gilbert, J.A., 2015. The soil microbiome influences grapevine-associated microbiota. mBio 6 (2). https://doi.org/10.1128/mBio.02527-14.

Zelenev, V.V., Van Bruggen, A.H.C., Leffelaar, P.A., Bloem, J., Semenov, A.M., 2006. Oscillating dynamics of bacterial populations and their predators in response to fresh organic matter added to soil: the simulation model 'BACWAVE-WEB. Soil Biology and Biochemistry 38 (7), 1690–1711. https://doi.org/10.1016/j.soilbio.2005.11.024.

Zhang, X., Xie, Z., Ma, Z., Barron-Gafford, G.A., Scott, R.L., Niu, G., 2022. A microbial-explicit soil organic carbon decomposition model (MESDM): development and testing at a semiarid grassland site. Journal of Advances in Modeling Earth Systems 14 (1), e2021MS002485. https://doi.org/10.1029/2021MS002485.